University of Tartu

Faculty of Science and Technology

Institute of Physics

Toomas Daniel Viskus

Resistive switching in HfO_2 - TiO_2 thin films

Master's Thesis (30 EAP)

Supervisors: Kaupo Kukli, PhD

Joonas Merisalu, MSc

Tartu 2024

Abstract

In this work resistive switching properties of samples where HfO_2:TiO_2 9.1 to 24 nm thick thin films of different HfO_2/TiO_2 ratios were deposited via atomic layer deposition on to a RuO_2 bottom electrode. The Pt top electrodes were deposited through a shadow-mask using electron beam evaporation and the RuO_2 bottom electrode was deposited using a chemical vapour deposition method. Samples with two different HfO_2:TiO_2 thin film thicknesses were prepared for each ratio and annealed samples were also prepared. X-ray diffraction analysis showed that samples with a low HfO_2/ TiO_2 ratio exhibited strong rutile phase reflexes while samples with a high HfO_2/ TiO_2 ratio exhibited strong monoclinic phase reflexes. A strong resemblance to orthorhombic $HfTiO_4$ phase was shown in samples with intermediate HfO_2/TiO_2 ratios. Preliminary I-V curve measurements showed that 24 samples demonstrated resistive switching behaviour although resistive switching performance varied significantly from sample to sample. The best performing, the most representative, samples were investigated more thoroughly. The samples demonstrated good endurance properties showing up to 3000 resistive switching cycles with memory window values (low resistive state and high resistive state ratio) of over 10. The samples also showed excellent retention, lasting up to 6 hours at both room temperature and at 110 °C. The best performing sample even withstood 6-hour long measurements at 140 °C. In addition to this it was shown that changing the pulse length of the applied voltage had a significant effect on the stability of resistive switching in the samples. Based on this work it can be said that HfO_2:TiO_2 thin films with a RuO_2 bottom electrode and Ti top electrode are promising candidate materials for memory applications.

CERC: P250 (Condensed matter: structure, thermal and mechanical properties, crystallography, phase equilibria) and P260 (Condensed matter: structure, thermal and mechanical properties, crystallography, phase equilibria)

Abstrakt

Käesolevas töös uuriti takistuslülitusnähtust objektides, kus 9.1–24 nm paksused HfO_2:TiO_2 kiled sadestati RuO_2 alumisele elektroodile. Pealmised Pt punktelektroodid sadestati läbi füüsilise maski elektronkiiraurustus-meetodiga ja alumine RuO_2 elektrood sadestati keemilise aurufaassadestus-meetodiga erineva HfO_2/TiO_2 suhtega kile jaoks valmistati kahe erineva paksusega objekti ning iga objekti jaoks tehti ka lõõmutatud teisikeksemplar. Röntgendifraktsioon analüüs näitas, et madala HfO_2/TiO_2 suhtega objektides esinesid tugevad TiO_2 rutiili faasi refleksid ja kõrge HfO_2/TiO_2 suhtega objektides esinesid tugevad HfO_2 monokliinse faasi refleksid. Vahepealsetes HfO_2/TiO_2 suhtega objektides oli näha sarnasusi $HfTiO_4$ ortorombilise faasiga. Esmaste volt-amper kõverate mõõtmistel esines takistuslülitusnähtus 24 objektis kuigi, lülitumisparameetrid varieerusid märgatavalt objektide vahel. Kõige paremini lülituvad, kõige eristuvamaid, objekte uuriti põhjalikumalt. Objektidel esinesid ka head vastupidavus omadused. Neilt oli võimalik mõõta kuni 3000 takistuslülitustsüklit, kus mäluakna väärtus (madala ja kõrge takistusega olekute voolude suhe) oli üle 10. Objektidel esinesid ka suurepärased püsivusomadused, pidades vastu 6 tunni pikkuseid mõõtmisi nii toatemperatuuril kui ka 110 °C juures. Kõige vastupidavam objekt pidas 140 °C juures vastu 6 tundi. Lisaks sellele näidati, et objektidele rakendatava pinge pulsipikkuse muutmine avaldas märgatavat mõju takistuslülitmisele. Käesolevatöö põhjal võib öelda, et RuO_2 alumise elektroodiga ja Pt pealmise elektroodiga HfO_2:TiO_2 kiled on lubavad mälumaterjali kanditaadid.

CERC: P250 (Tahke aine: struktuur, termilised ja mehhaanilised omadused, kristallograafia, faaside tasakaalud) ja P260 (Tahke aine: elektrooniline struktuur, elektrilised, magnetilised ja optilised omadused, ülijuhtivus, magnetresonants, spektroskoopia)

Table of contents

1. Introduction ... 5

2. Description of resistive switching terms ... 6

3. Resistive switching mechanisms ... 8

4. Atomic layer deposition ... 10

5. Electron beam evaporation ... 14

6. X-ray diffraction analysis ... 16

7. Transmission electron microscopy ... 18

8. Hafnium(IV) oxide ... 19

9. Titanium(IV) oxide ... 21

10. Experimental ... 23

10.1. Sample preparation ... 23

10.2. Electrical measurements ... 25

11. Results and discussion ... 28

11.1. GIXRD ... 28

11.2. Transmission electron microscopy ... 29

11.3. Resistive switching ... 31

12. Comparison ... 40

13. Conclusion ... 42

References ... 43

1. Introduction

Resistive random-access memory (RRAM or ReRAM) is a type of non-volatile memory that takes advantage of the resistive switching phenomena observed in some materials to store information. The advantages of RRAM over other memory types are low operation voltage, low power consumption, high density (memory cells per unit of area). ReRAM also has the benefit of being compatible with current complementary metal oxide semiconductor (CMOS) manufacturing technology due to its simple metal-insulator-metal structure [1]. An industrially manufactured RRAM chip may consist of a crossbar matrix such as the one described by Kim et al.[2]. In this structure a dielectric material is deposited between the bottom and top bars. A single cell can be selected by applying voltage to the top bar while the selected cells bottom bar is grounded and the unselected bottom bars have a reverse bias applied to them. The main challenge in RRAM application is finding materials that have suitable switching characteristics. Many materials have been shown to exhibit resistive switching, this includes organic materials such as biological materials [3] and polymers [4] and inorganic materials such as metal oxides [5] of which the last ones are the focus of this master's thesis. The choice of top and bottom electrodes also plays an important role in the switching characteristics of the device. Both chemically inert and more active metals have been used as electrode materials. Examples of inert metals used include Au [6] and Pt [7]. Some active metals used as electrode materials are Ag[8] , Ni [9], Cu [10] etc. Nitrides such as TiN [11] and TaN [12] have also been used. Resistive switching has been previously studied in both TiO_2 [13], [14], [15] and HfO_2 [16], [17], [18]. Devices utilizing a TiO_2/HfO_2 bilayer have also been studied, whereas the number of studies focused on multilayered structures is scarce [19]. In this work I investigated devices with a Pt/HfO_2: TiO_2/RuO_2 structure where a $TiO_2:HfO_2$ layer is deposited on to a RuO_2 bottom electrode with a Pt top electrode.

2. Description of resistive switching terms

Resistive switching (RS) is a phenomenon where a dielectric material has more than one electrical resistance state. These different states can be achieved by applying electric fields with different polarities and strengths to the dielectric material. A resistive switching cell (also called a device) consists of a bottom electrode (BE), the resistive switching material and a top electrode (TE). The electric field is created by applying a potential to the TE and reference to ground is connected to the BE. The difference between resistive switching and dielectric breakdown is that resistive switching is a reversable process. To differentiate between different resistances states, the terms such as high resistive state (HRS) and low resistive state (LRS) are used. The difference between resistance values in LRS and HRS is called a memory window width. The memory window width can also be expressed as a quotient (I_{LRS}/I_{HRS}) of the current value in LRS (I_{LRS}) divided by the current value in HRS (I_{HRS}) at some specified voltage, e.g. 0.2 V. The initial soft breakdown of the dielectric material is called a forming process. The switching of a material from a HRS to a LRS is called a SET process and the switching from a LRS to a HRS is called a RESET process. Often a current compliance is applied during the SET process to avoid the dielectric breakdown of the material. When both a SET and RESET processes are consecutively applied then the material has undergone a RS cycle. Two different modes of switching have been noted, bipolar (Fig. 1 a) and unipolar (Fig. 1 b) switching. RS in a material is called unipolar when voltages of the same polarity but different amplitudes are required to achieve different resistance states. The term bipolar is used when both polarities are required to achieve different resistance states. Endurance describes how many RS cycles a cell can endure before a significant decrease or collapse in the memory window width. Retention expresses the amount of time a resistance state is stable. Repeatability describes how likely it is that a set of cells will behave similarly. [20]

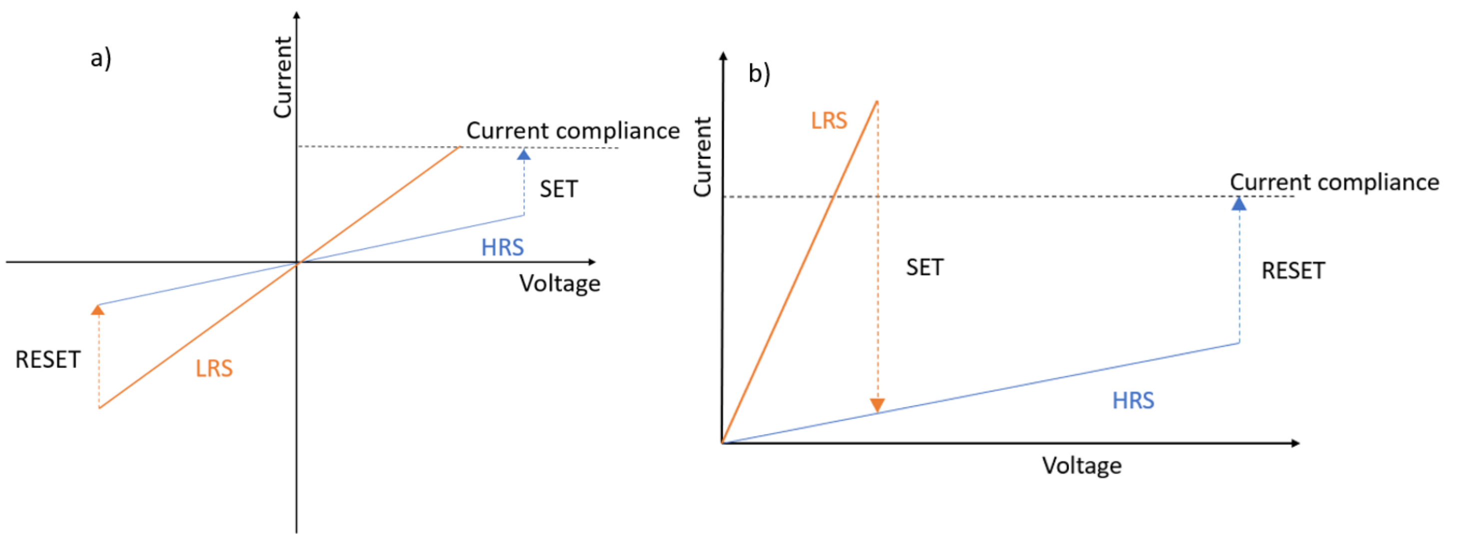

Fig. 1. schematic representation of Bipolar (a) and unipolar (b) switching on a graph.

3. Resistive switching mechanisms

There are three main RS mechanisms described in literature: electrochemical metallization (ECM), valance change mechanism (VCM) and the thermochemical mechanism (TCM). All these mechanisms attribute the change in resistance to the formation of a conductive filament (CF) within the resistive switching material which can be ruptured and then reconstructed by applying electric fields to the resistive switching material. The electrode materials and resistive RS material play a major role in determining the resistive switching mechanism [21]. ECM and VCM are similar in that they both involve the transport of ion and electrochemical reactions. The difference is that the electrochemical reactions in ECM are based on migration of the cations of active metals such as Ag and Cu [6] while in VCM the reactions are based on the migration of oxygen vacancies in metal oxides. It is important to note that depending on the structure of a sample both mechanisms can contribute to resistive switching [22]. Since the samples investigated in this work are based on metal oxides and do not utilize active metals, the domination of the valance change mechanism is assumed. In this mechanism (Fig. 2 a) the RS is caused by the migration of oxygen vacancies present in the defective areas of non-stoichiometric metal oxide in RS material. The initial forming of this CF is attained by applying an electric field to an RS cell which causes a leakage current to flow through the cell. This causes Joule heating to take place due to the ohmic resistance of the material. A sufficiently strong electric field in the material aided by the elevated temperature causes oxygen vacancies to migrate towards the negatively biased electrode of the cell. As these vacancies migrate, they start to coalesce and combine with the metal oxide to form a more conductive sub-oxide phase. Under the influence of an electric field this conductive phase can form a filament that reaches from the top electrode to the bottom electrode causing a decrease of resistance, thereby switching the cell into a LRS. It is important to note that the initial forming of this CF in a pristine device requires a higher voltage than what is required in later switches. It is also reasonable to assume that this CF in more likely to begin forming around physical defects such as the grain boundaries between crystallites. In order to attain a HRS, the CF must be ruptured. In the case of bipolar switching this occurs when a opposite bias is applied to the electrode which causes oxygen vacancies to migrate away from said electrode and the CF to be ruptured (Fig. 2 b). This rupture causes an increase in resistance, thereby switching the device into a HRS. To restore the CF, the electric field is again flipped, and the oxygen vacancies migrate back to the filament. In unipolar switching the HRS is achieved when the CF is ruptured due to excessive

Joule heating caused by the higher current running through the device at a low resistance state [21]. This whole process of switching between resistance states can take as little as 5 ns depending on the material [23].

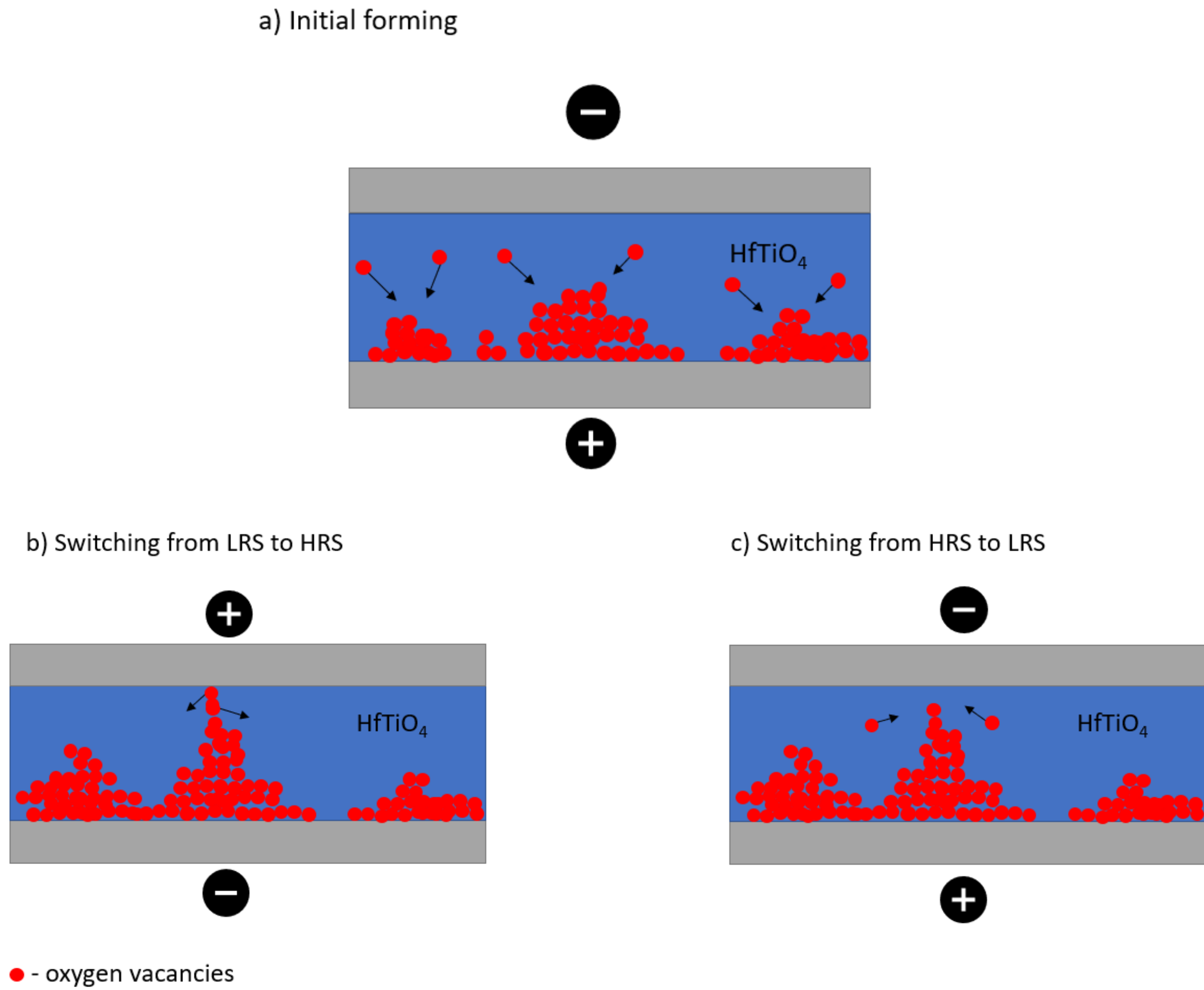

Fig. 2. Schematic representation of a) initial forming, b) switching from LRS to HRS and c) switching back from HRS to LRS.

4. Atomic layer deposition

Atomic layer deposition (ALD) is a thin film deposition method that can be used to deposit both chemically and structurally uniform films on to a substrate. ALD is suitable for covering both comparatively even surfaces and surfaces that have more complex details such as trenches. ALD can be considered a variation of chemical vapor deposition (CVD). The difference between the two is that in ALD the precursors are introduced into the deposition chamber at different sequences while in CVD the precursors are injected at the same time. The process of injecting a precursor into the deposition chamber is called a precursor pulse and the length of time which the precursor gas is allowed to flow into the chamber is referred to as the precursor pulse length. Each precursor pulse is followed by a purge pulse, where an inert gas flows into the deposition chamber to remove any precursor molecules that did not react with the substrate surface. In ALD, when a precursor is injected into the chamber it reacts with the chemically active OH-groups on the surface of the substrate. Once the precursor has reacted with the chemically active groups on the surface the chamber is purged, and the second precursor is pumped into the chamber. The point of the second precursor is for it to react with the newly formed surface groups in such a way that creates the desired substance and a new chemically active groups that the first precursor molecules can then react with again. This self-limiting growth mechanism allows for the film to be grown layer-by-layer which allows for excellent control over the thickness of the film (Fig. 3). Typically, an inert carrier gas such as N_2 is used to guide the precursor chemicals into the chamber. Supercycles are applied to create a thinfilm of laminate layers or a mixture of materials. A supercycle consists of multiple different material ALD cycles. For example, in this work supercycles with a formula of was $X \times (Y \times [TiCl_4 + H_2O] + Z \times [HfCl_4 + H_2O])$ were applied to grow the HfO_2:TiO_2 thin film. [24]

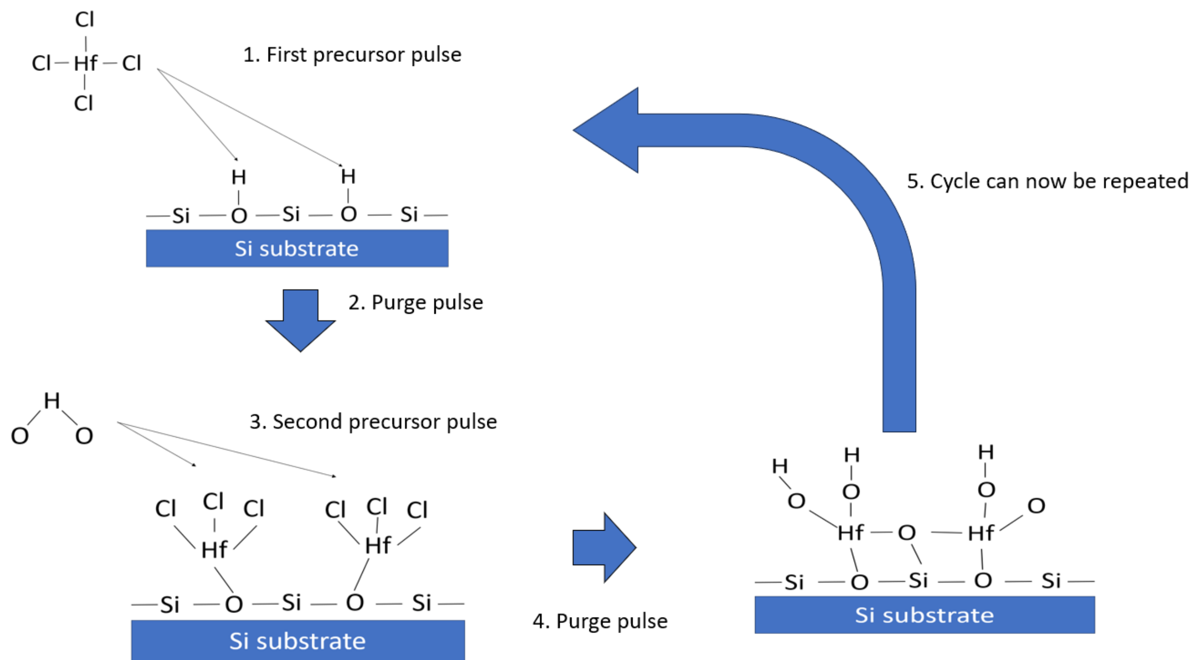

Fig. 3. Schematic representation of an ALD cycle where $HfCl_4$ and H_2O are used to deposit a layer of HfO_2.

In the case of DRAM memory cells trenches are deep holes that have been etched into a substrate. When filled with a dielectric material these trenches can be used as capacitors to store a charge. Whether the capacitor is charged or not can be interpreted as a bit “0” or “1” . For the DRAM cell to work properly the dielectric material covering the trench walls must be as uniform as possible and for this reason ALD is most likely the only suitable deposition method for the task [24].

The main limitations of ALD are slow growth speeds and chemical impurities which can be unacceptable for some applications. For example, the growth rate of metal oxides such as TiO_2 and HfO_2 grown via ALD can vary but is typically around 1 Å/cycle and each cycle can take as long as 30 sec [25], [26].Using a physical vapour deposition (PVD) method such as electron beam evaporation one can achieve growth rates of about 2 Å/sec when depositing TiO_2 [27] and 0.5 2 Å/sec when depositing HfO_2 [28].When comparing thinfilms deposited with methods PVD method with ones produced via ALD, the ALD films tend to have more impurities since the chemical reactions that produce the films do not go entirely to completion. This issue occurs in other CVD methods as well. The superior purity of PVD films comes from the lack of chemical processes when depositing the film. In PVD the film is deposited by sublimation of the source material via heating, ion beam or laser beam. If the

deposition chamber is under high vacuum and no contaminants are present, then the deposited film should be as pure as the source material. Growth rate in ALD can vary depending on the deposited material but the typical growth rate is some tens of nanometres per second. This means that ALD is useful in nanoelectronics where the film thicknesses are below 100 nm but has limited usefulness in applications where film thicknesses in the micrometre range are required. [24]

Ideally one atomic layer of material should be deposited during each ALD cycle, however this is often not the case. There are three different growth modes described in ALD for different deposition surfaces. These growth modes carry the names of those who first described them: Volmer-Weber (Fig. 4 a), Stranski-Krastanov (Fig. 4 b) and Frank-Van der Merwe (Fig. 4 c). In the case of Volmer-Weber the first ALD cycles produce clusters of material around nucleation centres. As more ALD cycles are applied the clusters grow in size and crystallization may start to appear until the cluster becomes large enough that they merge into a single polycrystalline film. This growth mode prevails when the bond between the particles that make up the thinfilm are stronger than those between the particles and the substrate. The Stranski-Krastanov growth mode start off with the formation of single monolayers of material that cover the surface of the substrate and as the film continues to grow, islands start to form on the film. This growth mode most likely occurs due to the presence of small but noticeable differences in the crystal lattice of the substrate material and the thin film. At first the crystal structure of the thin film is heavily influence by the crystal structure of the substrate and tension forms within the thin film. As the film continues to grow a relaxation of tension occurs and the crystal lattice of the film starts to follow its own energy minimums which in turn causes the film to grow as islands rather than homogenous monolayers. Frank-Van der Merwe is the most orderly growth mode. In this case the film grows monolayer by monolayer and each new layer is less energetically affected by the substrate than the last. This growth mode is most likely to occur when the crystal lattice

parameters of the substrate and the film are quite similar. [29]

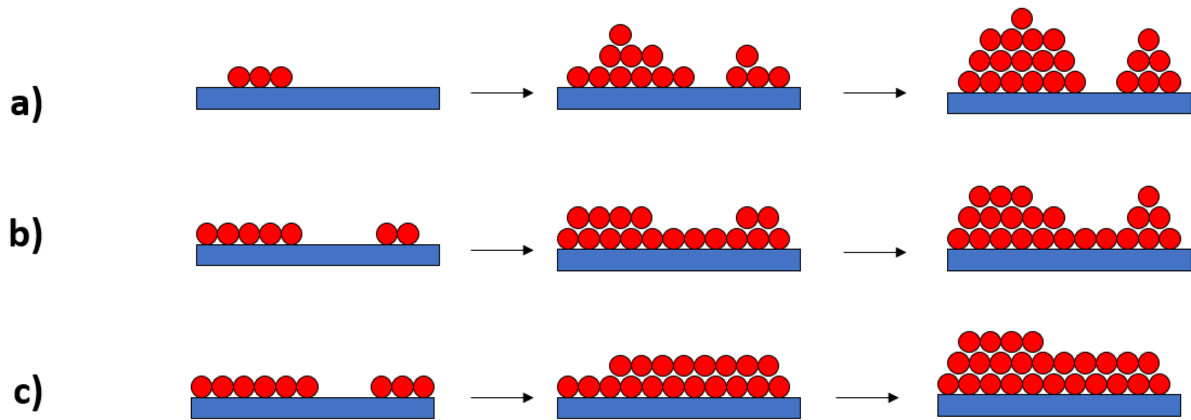

Fig. 4. Schematic representation of Volmer-Weber (a), Stranski-Krastanov (b) and Frank-Van der Merwe (c) growth modes.

Out of the three growth modes the Wolmer-Weber growth mode is most likely to occur since the other modes require some degree of similarity between substrate and thin film the crystal latices, which is not likely occur unless specifically intended [30]. This sort of unorderly growth mode causes the grown film to be much more defective than an ideal monolayer-by-monolayer grown film. The boundary layers present in the polycrystalline film cause leakage currents, reduction of the band gap and changes in the dielectric value of the material. The Wolmer-Weber growth mode also causes the formation of a transition layer between the substrate and the film that has an unpredictable composition and properties.

5. Electron beam evaporation

Electron beam evaporation (EBE) (Fig. 5) is a physical vapor deposition method. In this method, a source material is placed inside of a copper crucible and then sublimated via the use of an electron beam. The crucible has a positive bias applied and is water cooled to avoid the evaporation of crucible material. To avoid excessive heat loss to the crucible a heat insulating material can be used. The electron source is usually a tungsten filament that is heated up so that thermionic emission occurs. The electron source is placed away from the line of sight of the crucible to avoid the deposition of source material on to the electron source. Magnetic fields are used to focus the electron beam onto the source material. The surface at which the beam is directed at is called the target. The emitted electrons are passed through an accelerator to give them the kinetic energy required to properly heat up the target surface and cause evaporation of the material. The evaporated atoms can interact with the electron beam and become positively charged ions that later move to the negatively biased substrate and absorb there. The deposition chamber is kept under high vacuum during deposition. This is done to minimize the scattering of electrons and ions from air molecules and protect the filament that would otherwise burn out due to reactions with oxygen in the air. High vacuum also helps to ensure the purity of the thin film since reactions between ions and air molecules are minimized.

One of the advantages of EBE when compared with other thermal deposition methods is that a wider selection of materials can be deposited. Both high and low melting point metals can be deposited as well as reactive metals. The ability to deposit high melting point metals comes from the localized heating of source materials thanks to the electron beam. This means that the crucible itself does not have to withstand the high temperatures required to deposit some metals and contamination is not an issue. Another advantage of EBE is that the deposited film is as pure as the source material. Purity of the source material is also important for even growth since impurities with higher vapor pressure than the source material can evaporate and cause a sudden burst of pressure that knocks large particles loose and onto the substrate. Film uniformity is also affected by deposition rate. If the deposition rate is high then the evaporated atoms can form clusters that can deposit in such a manner as to form pores in the thin film. One downside to EBE is that it is a line of sight method which means that it is unsuitable for covering more complex surface structures (e.g. the walls of trenches). [31]

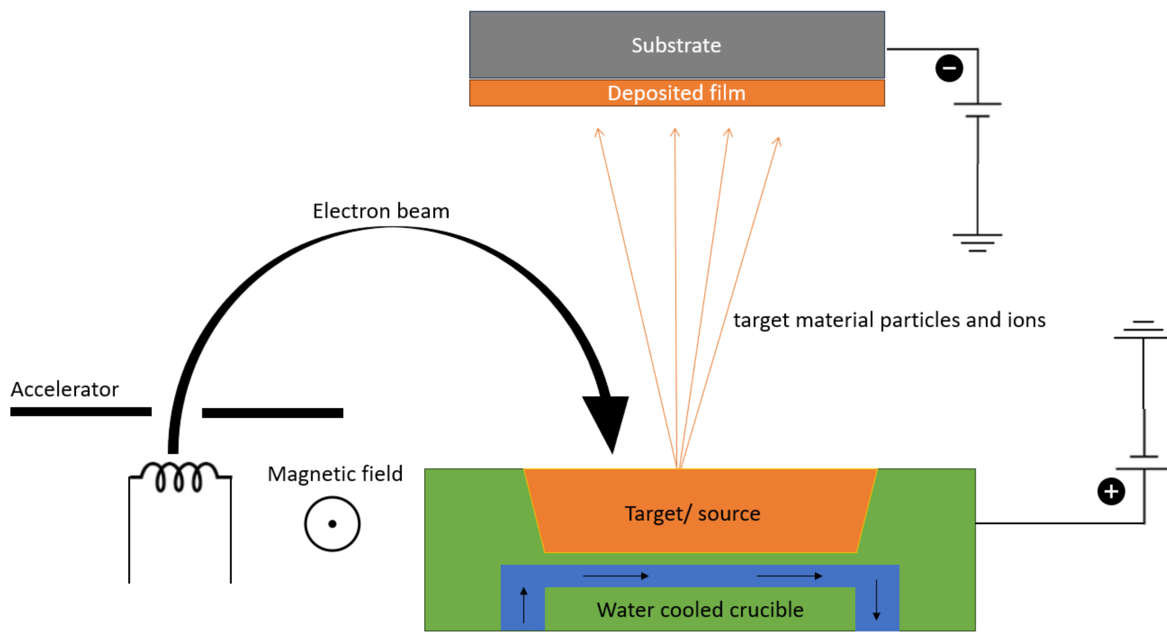

Fig. 5. schematic representation of an electron beam evaporator.

6. X-ray diffraction analysis

X-ray diffraction is an analysis method that allows for the investigation of a materials properties such as its atomic ordering, phase composition and some mechanical properties like stress in the material. The main equation used in X-ray diffraction is Braggs law (Equation 1.)

$$n\lambda = 2d_{hkl}\sin(\theta)$$

Equation 1. Where n is the diffraction order, λ is the wavelength, d_{hkl} is the distance between two parallel crystal lattice plains with the miller indexes h k l and θ is the angle of incidence.

Constructive interference occurs when X-rays falling onto a set of parallel lattice plains (h k l) with an angle of incidence θ have a difference in path length equal to a multiple of their wavelength λ. When using an X-ray source with a known wavelength we can scan a range of incidence angles and deduce the distance between parallel lattice plains. If the atoms of the sample under investigation have formed a crystal lattice, then sudden increases in intensity will be present on a diffractogram at certain angles of θ. In X-ray diffraction, these sudden increases in intensity are called reflexes.

In this work, grazing incidence X-ray diffraction (GIXRD) was used to investigate the crystallinity of the samples. In GIXRD the angle of incidence is kept constant at a set value bellow 1° while the detector scans a set range of 2θ angles while measuring the change in intensity. This differs from the widely used Bragg-Brentano configuration where that angles of incidence are higher and both the detector and source scan over the set range of 2θ angles. This configuration was not used since the higher angles of incidence means that the X-rays penetrate through the thinfilms into the substrate material resulting in a weak signal from the thin film and a strong signal from the substrate. Using GIXRD configuration mitigates this issue since the smaller angles of incidence cause less penetration into the substrate and an increase in the surface area from which the signal is collected. Collimator plates are used to block out X-rays that are not approaching the sample at the desired angle. This helps to decrease noise that results from stray X-rays thereby increasing resolution but has the downside of decreasing the intensity of reflexes due to fewer X-rays reaching the sample and detector (Fig. 6). When using GIXRD, calculation corrections must be used that consider the asymmetric geometry of this configuration. [32]

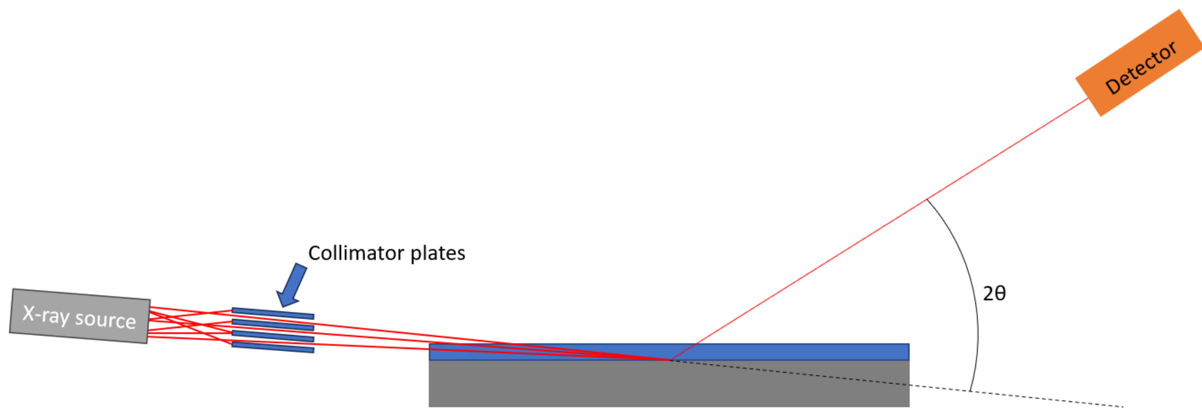

Fig. 6. Schematic representation of GIXRD configuration

7. Transmission electron microscopy

Transmission electron microscopy (TEM) is a material analysis method that uses high energy electrons to gather information about the elemental composition and compose and image of a sample. The samples themselves are generally quite thin, in the range of 100 nm, as to avoid excess scattering from the sample. In a TEM the electrons are generated via thermionic emission typically from a tungsten filament. Before interacting with the sample these electrons pass through a set of coils and plates called condenser lenses that use magnetic and electric fields to accelerate the electrons and focus them into a beam. When passing through the sample, some of the electrons are scattered. Both the primary beam and the scattered beams are directed through an objective lens that again focuses the beams and directs them through the objective aperture. Following the aperture is a set of projection lenses that magnify and focus the image onto a detector producing the final image. How the electrons interact with the sample determines the kind of information that is received. Elastic scattering from the sample produces diffraction patterns that give information about the structure of the sample. Inelastic scattering gives information about element composition and defects such as grain boundaries. The conventional operation mode for TEM is bright-field imaging, where only the primary beam is allowed to pass through the aperture. This operation mode gives information about the structure and morphology of the sample. Another operation mode, dark-field imaging utilises only diffracted beams giving better contrast for defects and heavier elements. Diffraction patterns can also be gathered to gain information about the crystal structure and crystallite orientation in polycrystalline samples. Elemental analysis can also be done via X-ray energy dispersive analysis. If an electron with high enough energy interacts with one of the sample atoms inner shell electrons, it can cause the ejection of an electron from said shell, leaving behind a vacancy and causing the atom to be in an excited state. In order to return to a stable state, one of the outer shell electrons moves to fill the inner shell vacancy, emitting an photon in the prosses. The energy of this photon is equal to the electron transition energy between the two electron states and these energies are characteristic to the element atom. [29]

8. Hafnium(IV) oxide

Hafnium(IV) oxide is a transition metal oxide that when deposited via ALD can form different crystalline phases: cubic, tetragonal, monoclinic and orthorhombic [33]. Hafnium(IV) oxide played a pivotal role in the advancement of nano-electronics. The demand for greater processing power at a lower cost required that the density of transistors on a single wafer needed to increase. This led to a rapid shrinking of a transistors dimensions. As the thickness of the gate dielectric shrank with the dimensions of the transistor, there was an increase in tunnelling current which eventually became a significant issue in the functioning of the transistor making them less efficient. Additionally, the decrease in the thickness of the dielectric meant that electrical breakdown became a greater risk [34].These issues could be solved by increasing the thickness of the gate dielectric, but this causes another problem to arise. Considering the gate electrode, the conduction channel and the dielectric in-between them forming a capacitor then according to equation 2.

$$C = \frac{\varepsilon_0 \varepsilon_r A}{d}$$

Equation 2 Where C is capacitance, $\varepsilon_r$is the relative permittivity of the dielectric material, ε_0 is the vacuum permittivity, A is the area of the electrode and d is the thickness of the dielectric material.

the increase in the thickness of the gate dielectric leads to a decrease in the capacitance and number of charge carriers in the conduction channel. This phenomenon meant that the κ-value of the commonly used SiO_2 ($\varepsilon \approx 4$ [35]) was no longer sufficient and another material with a higher κ-value was required [36]. A higher κ-value would allow for a thicker layer of dielectric to be deposited onto the conduction channel without loss in capacitance. For this application HfO_2 was a chosen since in addition to being a high- κ material ($\varepsilon \approx 25$ [35]) it also has a sufficient band gap that minimizes the conductance due to carrier injection. HfO_2 thin films also offer a large thermal budget due to being thermodynamically stable with SiO_2 at up to 900 °C. [37]. This is advantageous in chip manufacturing since the stability of various materials on the substrate must be considered.

RS has also been studied in HfO_2 thin films. Zhao *et al.* showed that multilevel RS occurs in TiN/HfO_2/Pt structures [38] where the HfO_2 thin film was deposited using reactive sputtering. Sokolov *et al*. have shown that resistive switching occurs in Ti/HfO_2/Pt structures where the HfO_2 thin film was deposited via ALD at 250 °C using tetrakis (ethyl-methyl-amino)

hafnium(IV) and water vapour as precursors [16]. HfO_2 is one of the most intensively studied material for RS, plausibly due to its wide use in the semiconductor industry [39], [40], [41].

9. Titanium(IV) oxide

Titanium(IV) oxide is a transition metal oxide that can occur in nature as the tetragonal rutile, anatase, orthorhombic brookite and in a monoclinic phase. At higher pressures it can also appear as TiO_2 (II) which as the PbO_2 and TiO_2(H) which has the hollandite structure [42].

The most well-known application of TiO_2 is in pigments, where its powdered form is used to produce white paint and is an additive in some foods and cosmetic products. TiO_2 thin films are a popular choice in dielectric mirrors due to the materials high refractive index, low absorption and ability to be combined with cheap materials such as SiO_2. Another popular use of TiO_2 thin films is in gas sensorics where the change in conductivity of the film due to absorbed gases is used to measure atmospheric conditions. TiO_2 thin films can be used to detect oxidative gases and reductive gases. The sensitivity and selectivity of the gas sensors can vary depending on the thin film thickness, porosity, grain size, doping metals and operating temperature.[43]

The refractive index of a TiO_2 thin film can vary, for example an amorphous thin film can have a refractive index in the range of 2.2 to 2.3 while a thin film with preferentially ordered crystallites in the anatase phase can have a refractive index up to 2.6 [44]. When TiO_2 is deposited using ALD it first forms an amorphous structure, as the film grows in thickness a crystalline phase begins to form. Crystallite size in the film increases as the thickness of the film is increased [45]. Crystallite size is also affected by growth temperature, films grown at lower temperatures form smaller crystallites [46]. Aarik et al. showed that films deposited using $TiCl_4$ and H_2O were amorphous at deposition temperatures below 165°C, anatase phase was present between temperatures of 165°C to 350°C after which rutile became the dominant phase [47] while Kukli et al. demonstrated that when using TiI_4 and H_2O_2 as precursors the rutile phase was also present at around 300°C [48]. Depending on the growth temperature refractive index of a TiO_2 thinfilm can also vary. Piercy *et al.* showed that at deposition temperatures ranging from 38 °C to 150 °C the refractive index of amorphous TiO_2 films varied from 2.3 to 2.45 [49].

RS has been shown in TiO_2 thinfilms. Oh et al. showed that resistive switching occurred in Pt/TiO_2/Pt devices where a 70 nm thick TiO_2 thin film was deposited using RF magnetron sputtering. It was also shown that RS occurred when the top electrode material was changed. Al, Ni. Ti and stainless steel were tested. [13]. Choi et al. [50] showed that resistive switching occurred in devices with a TiO_2 thin film deposited via ALD on to a Ru bottom electrode with

a Pt top electrode. Both unipolar and bipolar switching was demonstrated. The samples switched in both a clockwise and counterclockwise manner. The thickness of the TiO_2 thin films varied from 20 to 57 nm.

10. Experimental

10.1. Sample preparation

In this work the HfO_2:TiO_2 thin films were deposited using a homemade low-pressure flowtype ALD reactor (Fig. 7). The thin films were deposited onto a Si(1 0 0) substrate covered with a 10 nm thick TiN thin film. This substrate was manufactured by Fraunhofer IPMS in Dresden using a $TiCl_4$/NH_3 pulsed CVD method to produce the TiN film [51]. The metal precursors used were $HfCl_4$, $TiCl_4$, the oxygen precursor was H_2O and for carrier gas N_2 was used. The $TiCl_4$ and H_2O precursor sources were kept at room temperature outside the reactor. The HfO_2 precursor was kept in the chamber, and was heated up to 160 °C to achieve sufficient vapor pressure. Each ALD cycle started with a metal precursor pulse which was followed by an H_2O pulse. Each precursor pulse was followed by a pulse of carrier gas which purged the chamber. The time parameters were 5 s for the $HfCl_4$ pulse, 2 s for the $TiCl_4$ pulse and 2 s for the H_2O pulse. Each metal precursor pulse was followed by 2 s purge pulse and each H_2O pulse was followed by a 5 sec purge pulse. During deposition the substrate was kept at 350 °C. The bottom RuO_2 electrode was deposited using a CVD method described in Gatineau et al. [52]. The 60 nm thick Pt top electrodes material was deposited using electron beam sputtering. A shadow mask was used during the deposition of top electrodes to create circular electrodes with three different areas (0.204 mm^2, 0.052 mm^2 and 0.002mm^2) (Fig. 8). Multiple samples with varying TiO_2 to HfO_2 deposition cycles were prepared. For each ratio, samples with two different HfO_2:TiO_2 RS layer thicknesses were deposited. For each of these devices an annealed version was also prepared. Annealing was carried out at 400 °C for 30 min. HfO_2 reference samples were also prepared using 120 ($HfCl_4$ + H_2O) ALD cycles.

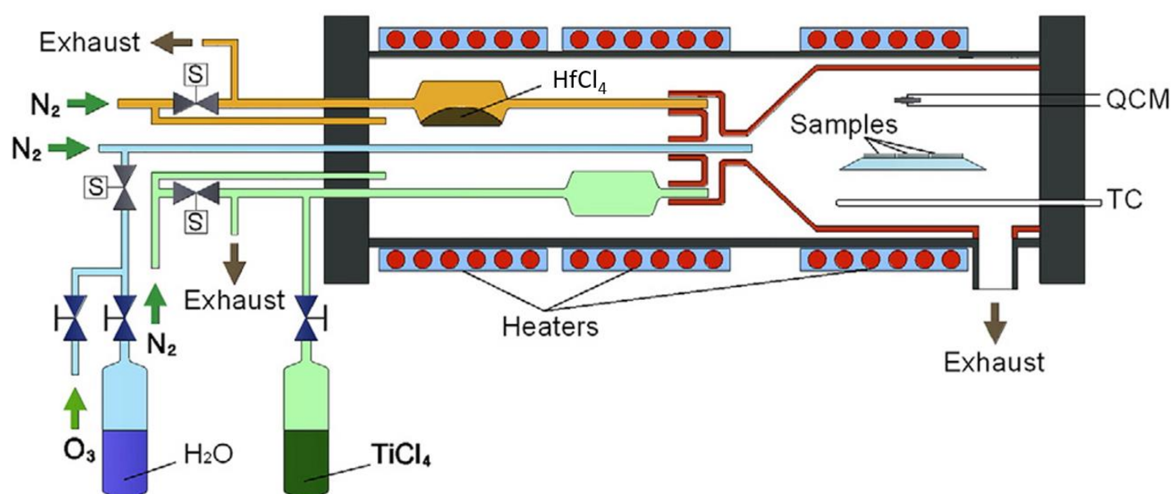

Fig. 7. Schematic representation of the ALD reactor set up used in this work. This figure has been adapted from a scientific article authored by Arroval et al.[53]

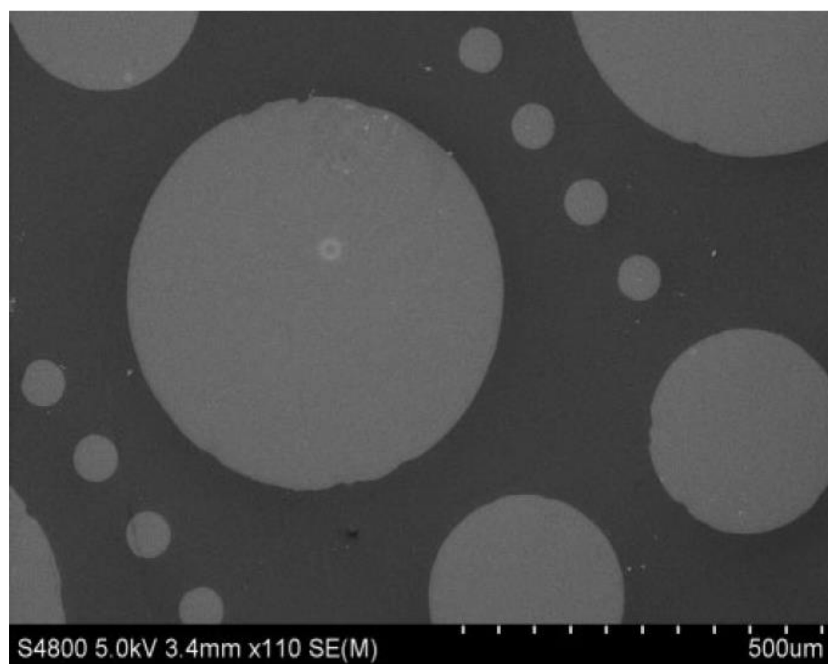

Fig. 8. Scanning electron microscope picture of circular top electrodes. The areas for the different areas are 0.204 mm^2 for the largest electrode, 0.052 mm^2 for the medium size electrode and 0.002mm^2 for the smallest electrode.

10.2. Electrical measurements

To investigate the resistive switching properties of the thin films a Cascade Microtech EPS150TRIAX probe station with at integrated Keithley 2636A source-meter was used at the University of Tartu thin films laboratory.

The sample was placed onto the base plate (chuck) of the probe station. To achieve contact with the bottom electrode a tungsten probe was pressed onto the bottom electrode contact located at the side of the sample. To assist this process, another tungsten probe was used to keep the sample from sliding away. To achieve contact with the top electrode, a thin gold wire attached to golden probe was used. The selected top electrode determined which cell on the sample was to be measured (Fig. 9) The source-meter was used to apply numerous voltage pulses that increased in amplitude by a set step until a given value was reached, after which the source-meter would start applying pulses that decreased in amplitude by the same step until a given value was reached.

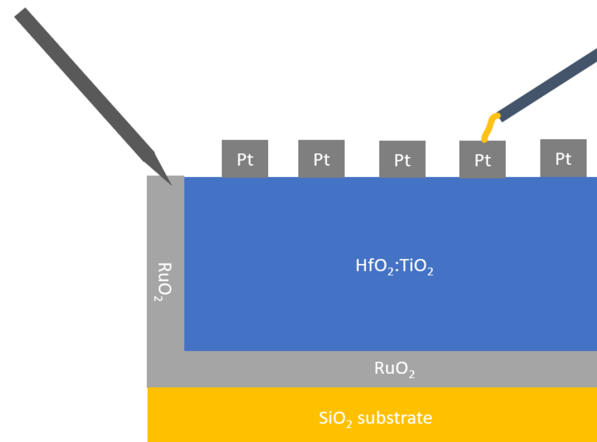

Fig. 9. Schematic representation of the measurement configuration used in this work.

The first step in the investigation was the formation of the conductive filament. This was done by applying a rather high voltage to the selected cell while also applying a current compliance to avoid the irreversible breakdown of the material. After the initial forming follows the RESET process in which the aim is to switch the cell into a high resistance state. To do this a voltage that was of the opposite polarity to the forming voltage was applied. After the initial RESET process followed the SET process where a voltage with the opposite polarity voltage was applied. Current compliance was also applied during the SET process.

To achieve proper switching in the cell some RS cycles with higher switching voltages were performed.

When the initial switches had been performed then the switching parameters were set and multiple switching cycles performed while the current was measured to produce I-V curves. Switching parameters were then tweaked based on these I-V curves. In the case of some samples this process of measuring I-V curves and then changing parameters was repeated multiple times. These final switching parameters were then used in endurance measurements. In endurance measurements the cell undergoes many switching cycles but instead of applying many voltage pulses to achieve a I-V curve only switching and reading voltage pulses were applied. The amplitude of the read voltage pulse (0.2 V) was much smaller than that of the switching voltages. This was done to ensure that the cell does not switch in response to the read voltage. The list of voltage pulses applied to a cell during endurance measurements was: first read voltage → first switching voltage → second read voltage → first read voltage on opposite polarity → second switching voltage → second read voltage on the opposite polarity (Fig. 10). This list of pulses was applied to the cell's multiple times and the current values were measured at the read voltages in both HRS and LRS states during each cycle are plotted on to a current vs number of RS cycles graph. Read voltage pulses on both the negative and positive polarity were used because the memory windows may not be perfectly symmetrical on opposite polarities. In this work the pulse length used in endurance measurements was 0.4 seconds with a wait time of 0.3 seconds.

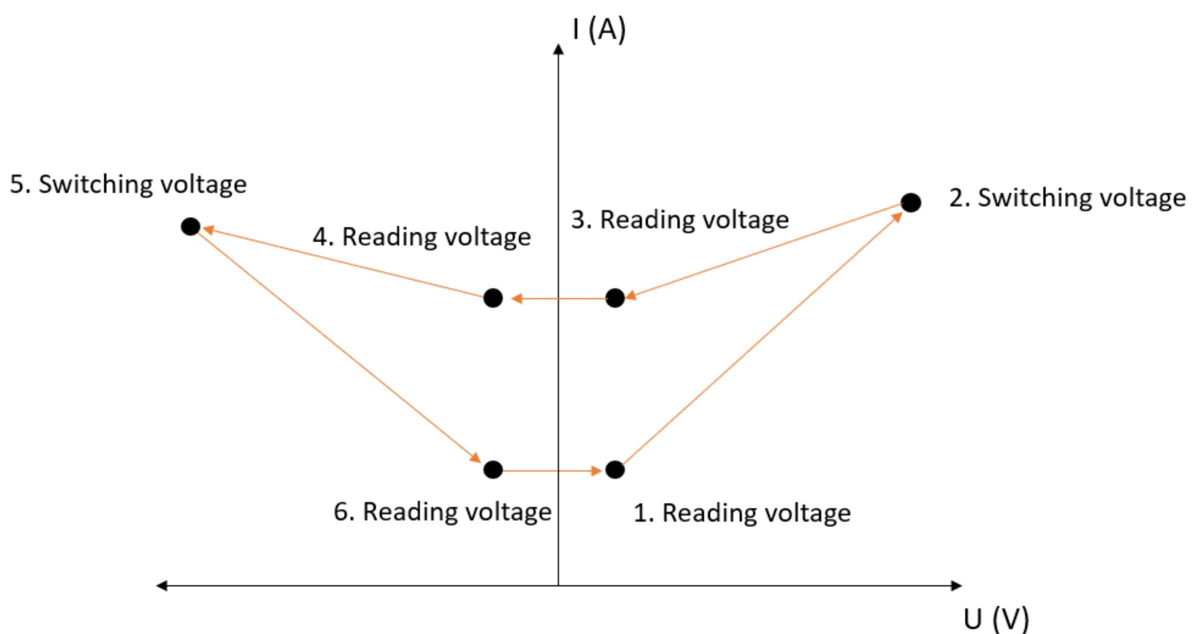

Fig. 10. Schematic representation of the list of pulses applied in a RS cycle during endurance measurements.

Before measuring retention, the initial I-V characteristics were measured to see the RS behaviour of the selected cell. These measurements were first carried out at room temperature and involved switching the cell into a certain state and then sequential read voltage pulses that were separated by a given time interval were applied for several hours. After the retention of one state was measured, the device was switched to the other state and the process was repeated. The current measured at the read voltages is plotted on a current VS time graph. If the memory window was stable, then the measurements were repeated at elevated temperatures. For measuring at elevated temperatures, the sample is heated using the base plate heating functionality. In this work the device was heated up to110 degrees Celsius. Before each temperature step additional I-V curves were measured to see if the elevated temperatures had affected the RS performance.

Repeatability measurements involved selecting several cells from the sample at random choice all over the top electrode matrix and applying the same parameters to all of them. In this work a simple repeatability test was performed on the samples where 10 cells were selected at random from the sample. The repeatability of the sample was then characterized by the number of cells that switched out of the ten tested cells.

For characterizing the material response to changes in pulse length I-V curves were measured using different pulse lengths. To better analyse the result a table is constructed with the information from these curves. This table consists of a memory window width, a standard deviation and a coefficient of variation column for each measured sample. Current compliance cannot be applied since the measuring equipment could not respond to the switching fast enough. As a result of this, lower SET voltages had to be applied to some cells to avoid irreversible breakdown. These measurements were carried out in Valladolid, Spain at the electricity and electronics department of the University of Valladolid. The measurement unit was a Keithley 4200-SCS semiconductor parameter analyser and the pulse measurements unit used was a Keithley 4225 PMU.

11. Results and discussion

11.1. GIXRD

GIXRD was used to determine phase composition. These measurements were carried out in a Smartlab model diffractogram produced by Rigaku. The angle of incidence was 0.42° with a tube power of 8.1 kW (Cu Kα radiation). The crystalline phases were identified using the database PDF-2 of the International Centre of Diffraction Data.

The GIXRD diffractograms (Fig. 11) showed that at low Hf/(Hf+Ti) relative cation ratio values one could observe a strong TiO_2 rutile reflex at about 27.5° and another smaller reflex at about 54.5°. As this ratio grows one can observe that the previously mentioned reflexes decrease in intensity and that new reflexes resembling $HfTiO_4$ orthorhombic start to form, the strongest of which are at about 24 ° and 31°. From the diffractograms one can see that at a cation ratio of 0.45 the $HfTiO_4$ orthorhombic phase has become dominant. A further growth in atomic ratio resulted in the appearance of HfO_2 monoclinic reflexes, this trend continued until no more $HfTiO_4$ orthorhombic reflexes were present, and the monoclinic phase had become completely dominant.

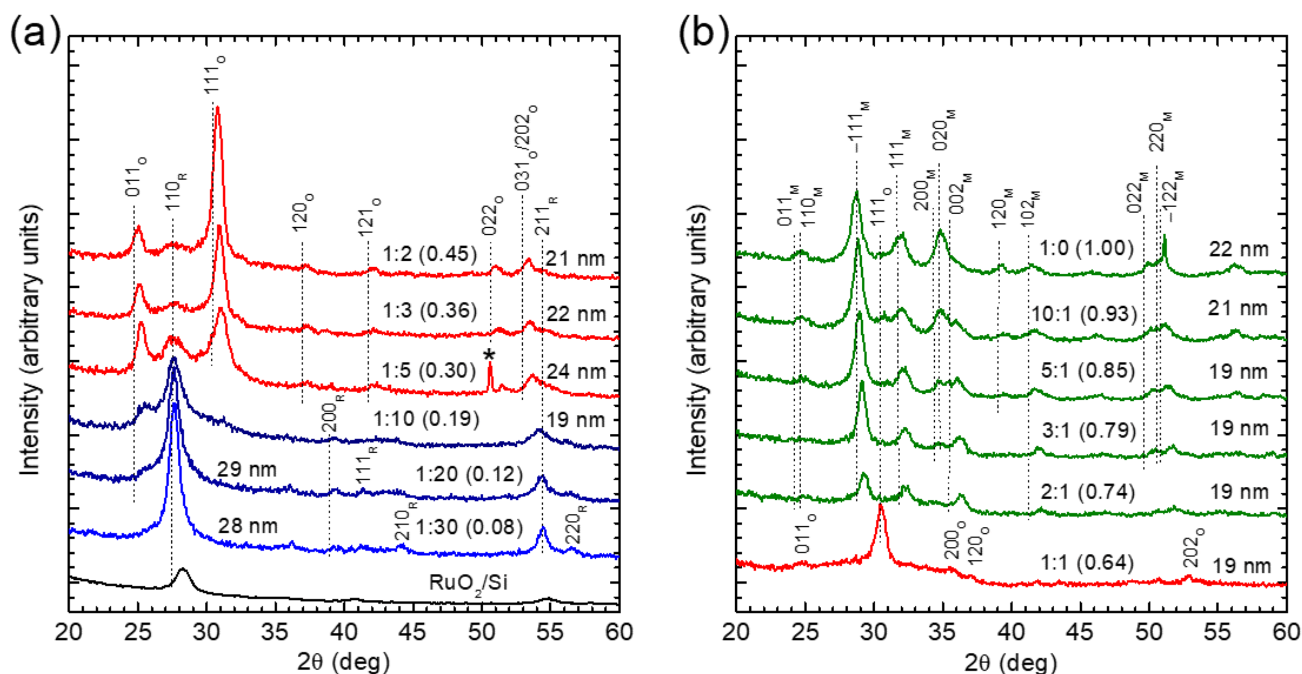

Fig. 11. GIXRD diffractograms gathered from the samples along with the corresponding HfO_2:TiO_2 cycle ratios, Hf/(Hf+Ti) relative cation rations and thickness of the measured film.

11.2. Transmission electron microscopy

Fig. 12 a shows a cross-sectional TEM picture taken from the sample where the 22 nm thick HfO_2:TiO_2 thin film was deposited using an ALD recipe of 80 × (3 × [$TiCl_4$ + H_2O] + 1 × [$HfCl_4$ + H_2O]). Between the Pt top electrode and the HfO_2:TiO_2 thinfilm there is a visible layer with an amorphous structure. EDX suggest that this layer is most likely empty and is caused by the separation of the Pt top electrode from the HfO_2:TiO_2 thin film during the TEM lamella preparation. The TEM picture also confirms the GIXRD result, showing that the HfO_2:TiO_2 layer is indeed crystalline in nature. The 5 nm thick RuO_2 bottom electrode is also visible and has formed a continuous layer covering the 10 nm thick TiN thin film with an interface layer in-between. A close-up of the HfO_2:TiO_2/ RuO_2/TiN interfaces (Fig. 13) shows that there are some crystallites that reach from the RuO_2 layer into the HfO_2:TiO_2 layer and some that reach from the TiN layer into the RuO_2 layer. It is unlikely that this is epitaxial growth since the RuO_2 bottom electrode is too thin to have developed its crystal structure. However, it is possible that the upper HfO_2:TiO_2 and lower TiN thin films affect the crystal lattice of the RuO_2 bottom electrode in such a manner that in some areas it conforms to the cubic TiN lattice and in others to the orthorhombic $HfTiO_4$ lattice. EDX analysis (Fig. 12 b, c, d) shows a high Ti concentration in the HfO_2:TiO_2 and the TiN thin films. A high concentration of Hf and Ru also seems to be present in the HfO_2:TiO_2 and Ru films respectively. EDX also suggest that there is a presence of all the mentioned elements in the Pt top electrode. Due to Pt being a heavier element , it is reasonable to assume that these elements are actually not present and what we are seeing is a continuum image artifact caused by the bremsstrahlung radiation coming from the Pt top electrode to be of a sufficient intensity as to be misinterpreted by the EDX as a signal coming from the analyte element [54].

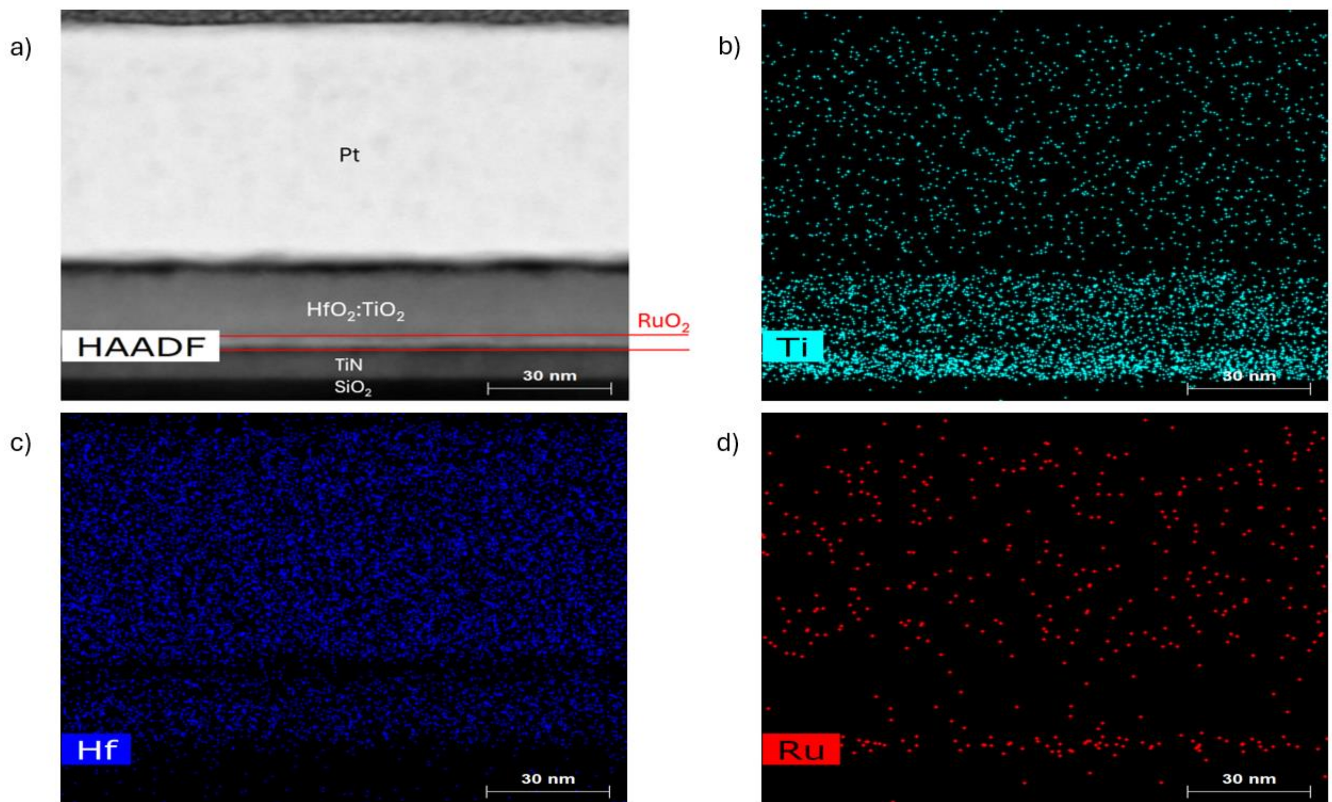

Fig. 12 TEM picture (a) of the sample where the $HfO_2:TiO_2$ thin film was deposited using an ALD recipe of 80 × (3 × [$TiCl_4$ + H_2O] + 1 × [$HfCl_4$ + H_2O]) along with EDX analysis for Ti (b), Hf (c) and Ru (d).

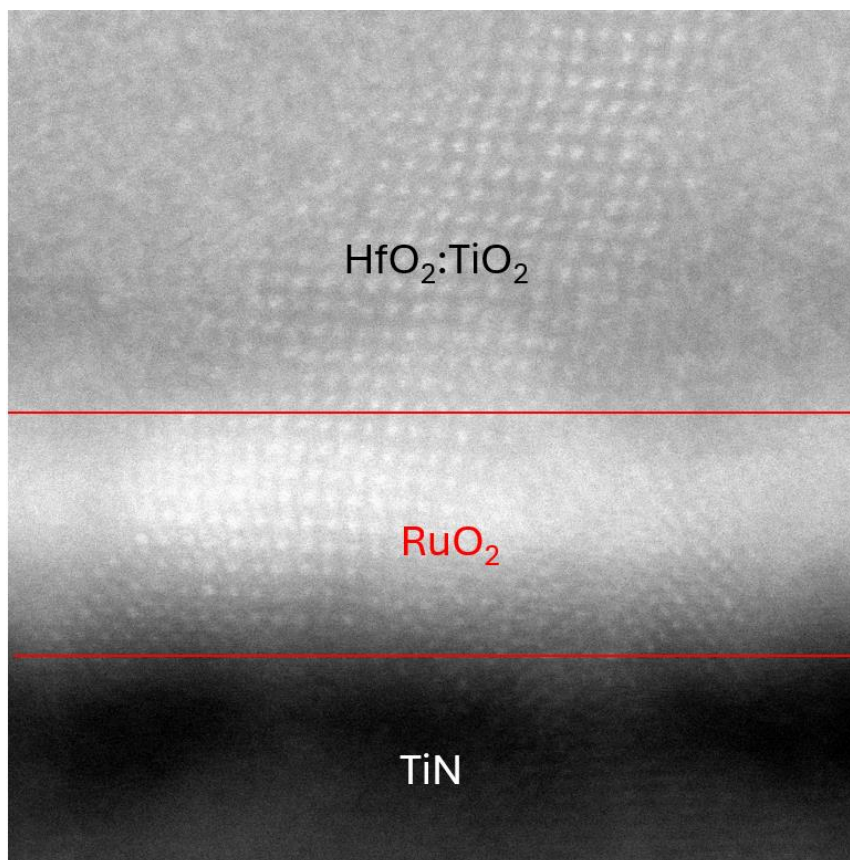

Fig. 13. TEM picture close-up of interface layers between the $HfO_2:TiO_2$ thin film and RuO_2 bottom electrode and the RuO_2 bottom electrode and TiN thin film. The $HfO_2:TiO_2$ thin film was deposited using an ALD recipe of 80 × (3 × [$TiCl_4$ + H_2O] + 1 × [$HfCl_4$ + H_2O])

11.3. Resistive switching

Preliminary I-V curve measurements showed that 24 samples demonstrated RS behaviour although RS performance characteristics such as memory window width, endurance and retention varied significantly from sample to sample. The best performing, the most representative, samples will be discussed here along with the reference samples. RS was shown in the samples where the HfO_2:TiO_2 thin film was deposited using 80 ALD supercycles with a HfO_2:TiO_2 deposition cycle ratio of 1:3. SET voltage values were between -1.1 V and -0.85 for the unannealed sample (Fig. 14 a) and, -1.4 V and -0.95 V for the annealed sample (Fig. 14 c.) The SET process for the unannealed sample consists of a sudden initial decrease in resistance followed by a more gradual process. This differs from the annealed sample which showed only a single sudden decrease in resistance. The RESET voltage values were between 1.1 V and 1.2 V for the unannealed sample (Fig. 14 a) and, 1.05 V and 1.25 V for the annealed sample (Fig. 14 c). Both samples had a RESET process where there was at first a sudden increase in resistance followed by a more gradual transition to HRS. The RESET voltage ranges indicated on the characteristics (Fig. 14 a and c) range from the initial decrease in current to a point where the current starts to increase once again. For the unannealed sample this initial RESET process was more stable when compared to the annealed device, for which it was difficult to discern the range of RESET voltages. Endurance graphs (Fig. 14 b, d) show that both samples had a similar memory window width. The unannealed sample (Fig. 14 b) demonstrated a good memory window for up to 3300 switching cycles. During the measurements the resistance in the HRS decreased in the first 800 cycles and then increased until it stabilised at about 1000 resistive switching cycles after which the memory window stayed stabilised for the rest of the test. The annealed sample (Fig. 14 d) initially showed a narrowing memory window but after about 500 cycles there was a sudden decrease in resistance in the LRS which caused the destabilisation of the HRS. This could have been caused by the RESET voltage no longer being sufficiently high to properly switch the device back into the HRS due to the increased current in the LRS.

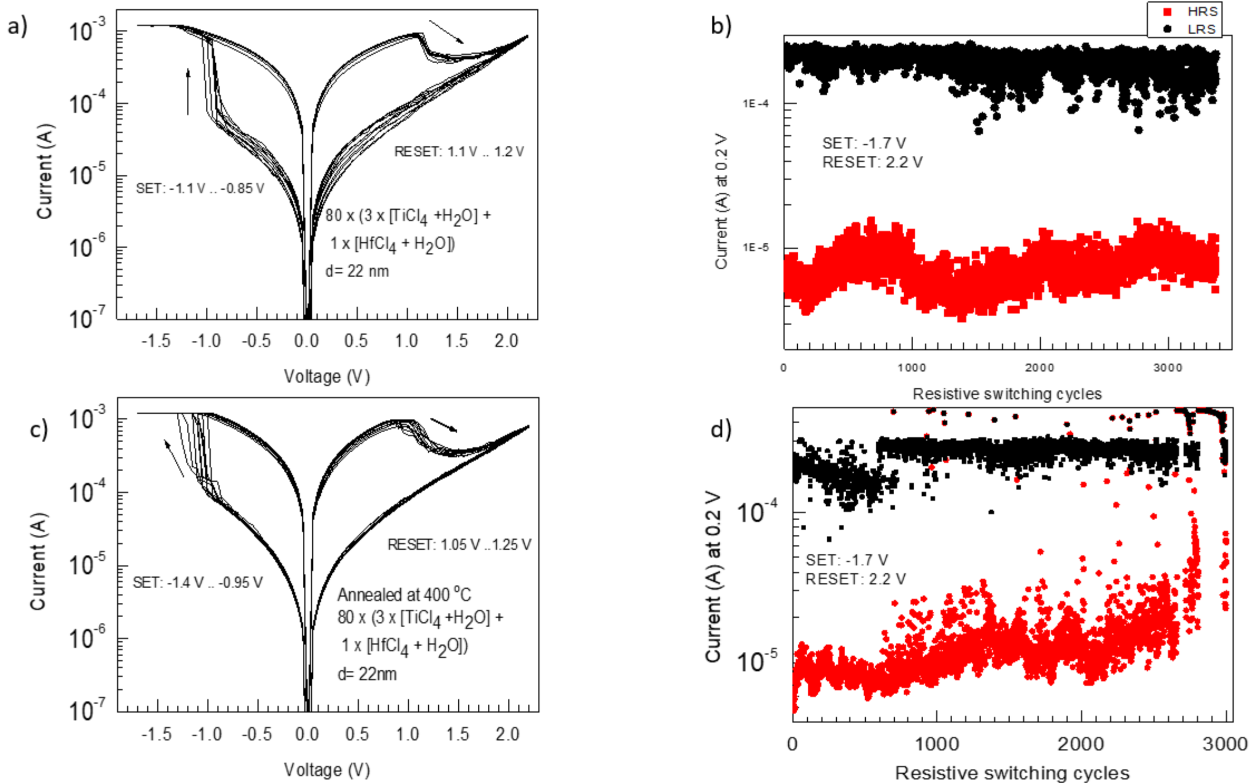

Fig. 14. I-V curves of an as-deposited sample (a) and an annealed sample (c) where the ALD recipe for the HfO_2:TiO_2 thin film was 80 × (3 × [$TiCl_4$ + H_2O] + 1 × [$HfCl_4$ + H_2O]) along with their endurance graphs (b, d).

Resistive switching was also shown in samples where the HfO_2: TiO_2 thin film with an ALD cycle ratio of 1:3 was deposited using 45 supercycles. The SET voltage values were between -0.85 V and -0.65 V for the unannealed sample and -1.0 V and -0.8 V for the annealed sample. The SET process in the unannealed sample had large and abrupt change in resistance followed by a much smaller gradual change in resistance than the samples deposited with 80 ALD supercycles. The annealed sample had a similar SET process to unannealed samples, except the abrupt change in resistance was somewhat smaller and the gradual change in resistance was larger. The RESET voltage values were between 0.9 – 1.35 V for the unannealed sample and, 1.55 – 1.7 V for the annealed sample. The unannealed sample had very gradual RESET process with almost no abrupt change in resistance, whereas the annealed sample had a large abrupt increase in resistance followed by a much smaller gradual increase in resistance. Endurance characteristics (Fig. 15 b, d) show that the annealed device (Fig. 15 b) had good stability throughout the endurance tests and there was even an increase in the memory window width during the first 600 resistive switching cycles after which the memory window stabilized. The annealed sample (Fig. 15 d) showed a rapid decrease in the memory window width during the first 200 resistive switching cycles. This was followed by about 1100 resistive switching cycles where the memory window was somewhat stable. From

about 1400 to 1600 there was a smooth decrease in memory window width. At about 2700 resistive switches the memory window widened due to a decrease in resistance in the LRS.

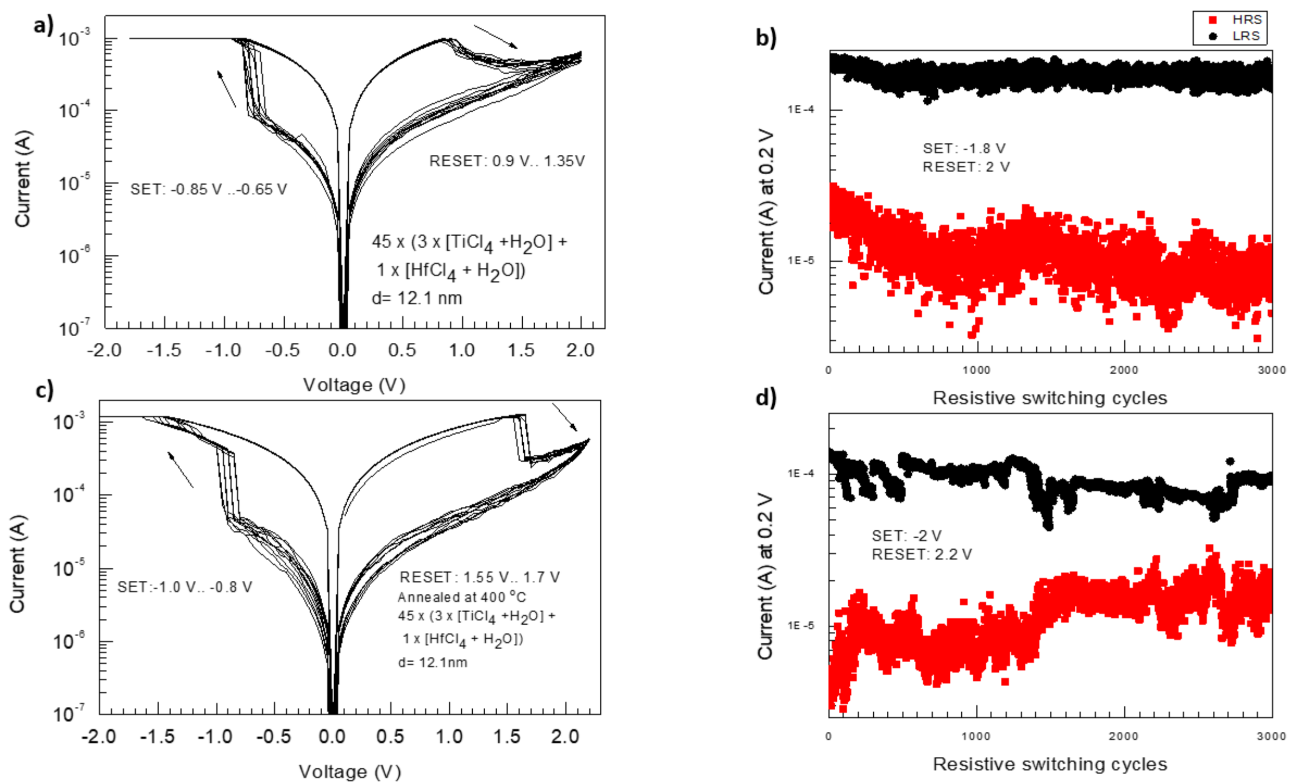

Fig. 15. I-V curves of an as-deposited sample (a) and an annealed sample (c) where the ALD recipe for the HfO_2:TiO_2 thin film was 45 × (3 × [$TiCl_4$ + H_2O] + 1 × [$HfCl_4$ + H_2O]) along with their corresponding endurance graphs (b, d).

Reference samples of HfO_2 showed resistive switching behaviour with the SET voltages for the annealed device ranged from -2.4 V to -1.2 V and RESET voltages varied from 2 V to 2.6 V (Fig. 16 a). Endurance could not be measured from this sample because the memory window for the sample collapsed during the I-V curve measurements. SET voltages for the unannealed device ranged from 1.2 V to 1.4 V and RESET voltages were between -1.1 V and -1.65 V (Fig. 16 b). The endurance characteristic for the unannealed device indicated that switching was somewhat stable for the first hundred RS cycles, after which the memory window began to shrink. After about 1000 RS cycles the memory window had collapsed almost completely. It should be noted that during I-V curve measurements both devices demonstrated some clockwise and counterclockwise switches, but the annealed sample had more stable switching in a clockwise manner and the unannealed device in a counter-clockwise manner. The coexistence of both clockwise and counterclockwise RS processes could be the reason why these samples performed poorly when compared with the samples of HfO_2:TiO_2 discussed above. Over the course of switching cycles some devices changed the switching direction between the clockwise and counterclockwise modes. In the Fig 16. c, it

can be noticed that during some RESET processes the current in HRS is higher than in the LRS suggesting that the device switched in a clockwise manner instead of the expected counterclockwise manner.

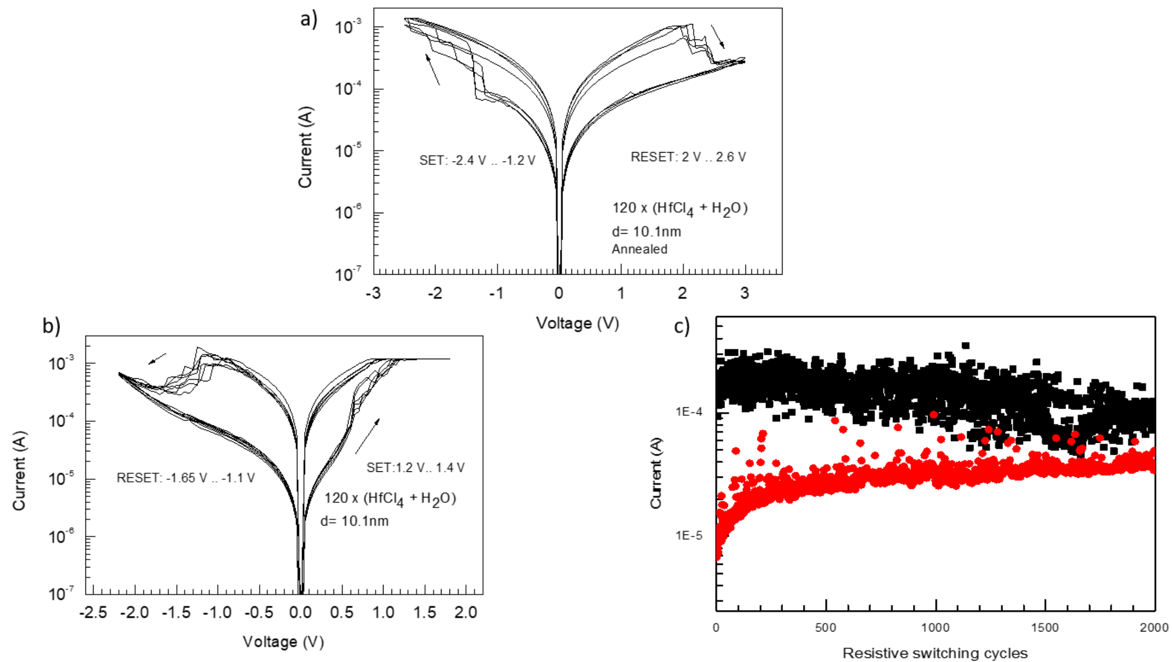

Fig. 16. I-V curves of an as-deposited sample (a) and an annealed sample (b) where the ALD recipe for the HfO_2 thin film was 120 × ($HfCl_4$ + H_2O) along with an endurance graph for the unannealed sample (c).

Retention measurements for these samples were carried out at both room temperature and 110 °C for 6 hours (Fig. 17). Unannealed samples where a HfO_2: TiO_2 thin film with a deposition cycle ratio of 1:3 was deposited using 80 supercycles showed a slight increase in resistance in the HRS during the first 1000 seconds of the test (Fig. 17 a) after which the state stabilized. A similar phenomenon can be observed for the annealed sample, but this change is more sudden (Fig. 17 b). Both the unannealed (Fig. 17 c) and annealed (Fig. 17 d) samples demonstrated good retention stability for the LRS at 110 °C. However, it can be argued that the annealed sample had somewhat more stable HRS compared to the unannealed sample. The noisier HRS of unannealed sample could be due to the movement of oxygen vacancies in and around the CF in response due to the temperature in conjunction with comparatively small positive read voltage that was applied to the cell.

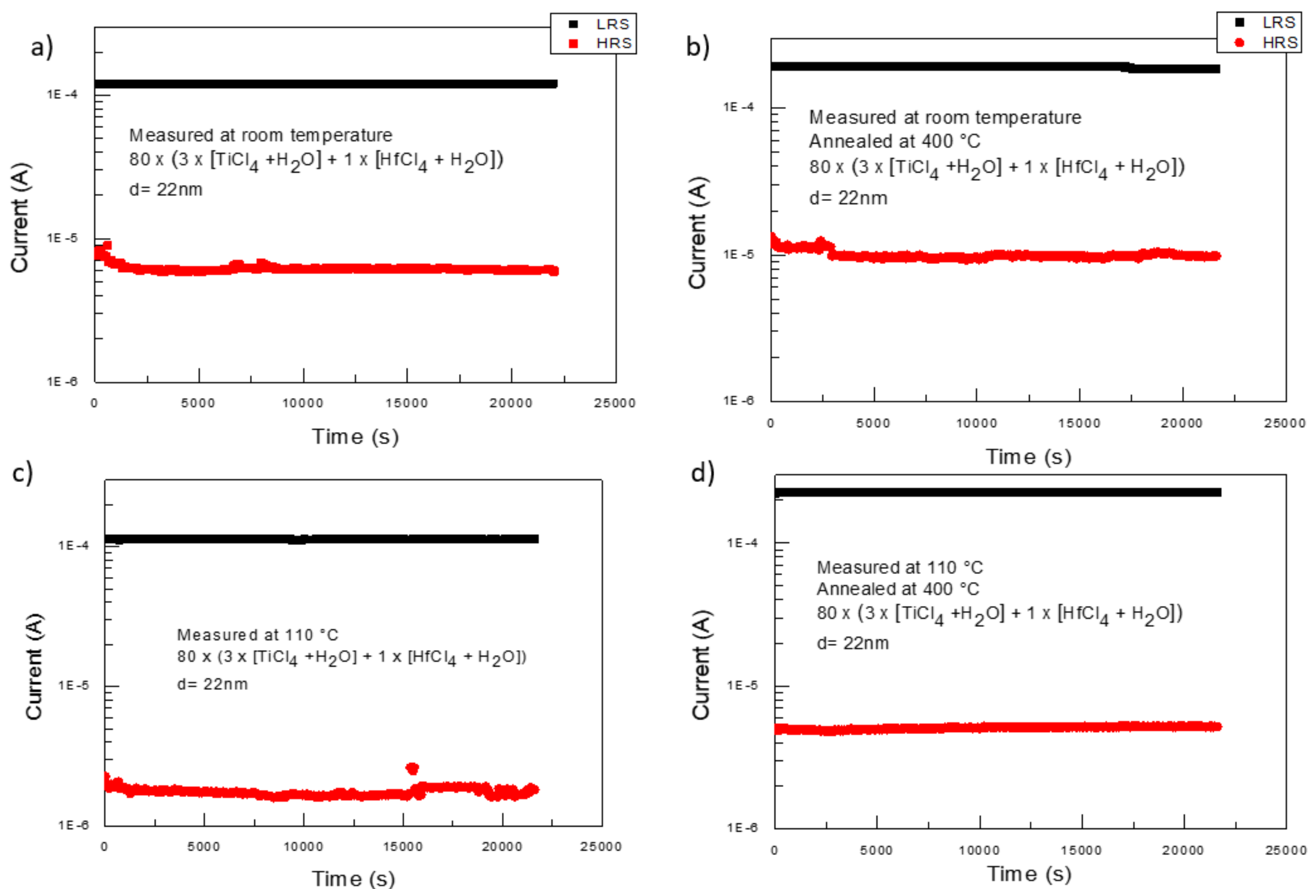

Fig. 17. Retention graphs at room temperature and 110 °C for both as-deposited (a, c) and annealed (b, d) samples with the ALD recipe of 80 × (3 × [$TiCl_4$ + H_2O] + 1 × [$HfCl_4$ + H_2O]).

Retention measurements were also carried out on devices where the 3:1 ALD cycle ratio HfO_2:TiO_2 thin film was deposited using 45 supercycles (Fig. 18) Both the unannealed and annealed samples demonstrated good stability at room temperature (Fig. 18 a) but showed notable instability when measuring at 110 °C. In the retention characteristic (Fig. 18 c) of unannealed sample measured at 110 °C there was initially a gradual increase in resistance over the first couple thousand of seconds. At about 7000 seconds there was a sudden decrease in resistance and 14000 seconds a sudden increase in resistance can be observed. During this period the resistance fluctuates erratically. After 14000 seconds the HRS became more stable but the resistance began decrease slightly. The annealed device (Fig. 18 d) demonstrated good stability in both the HRS and LRS for the first 13000 seconds after which the LRS begins to show signs of instability. After 17000 seconds both the HRS and LRS begin to destabilise,

both showing a very large increase in resistance during some read voltage pulses. However, this phenomenon has been noticed during some earlier measurements and is highly likely to be caused by a bad contact.

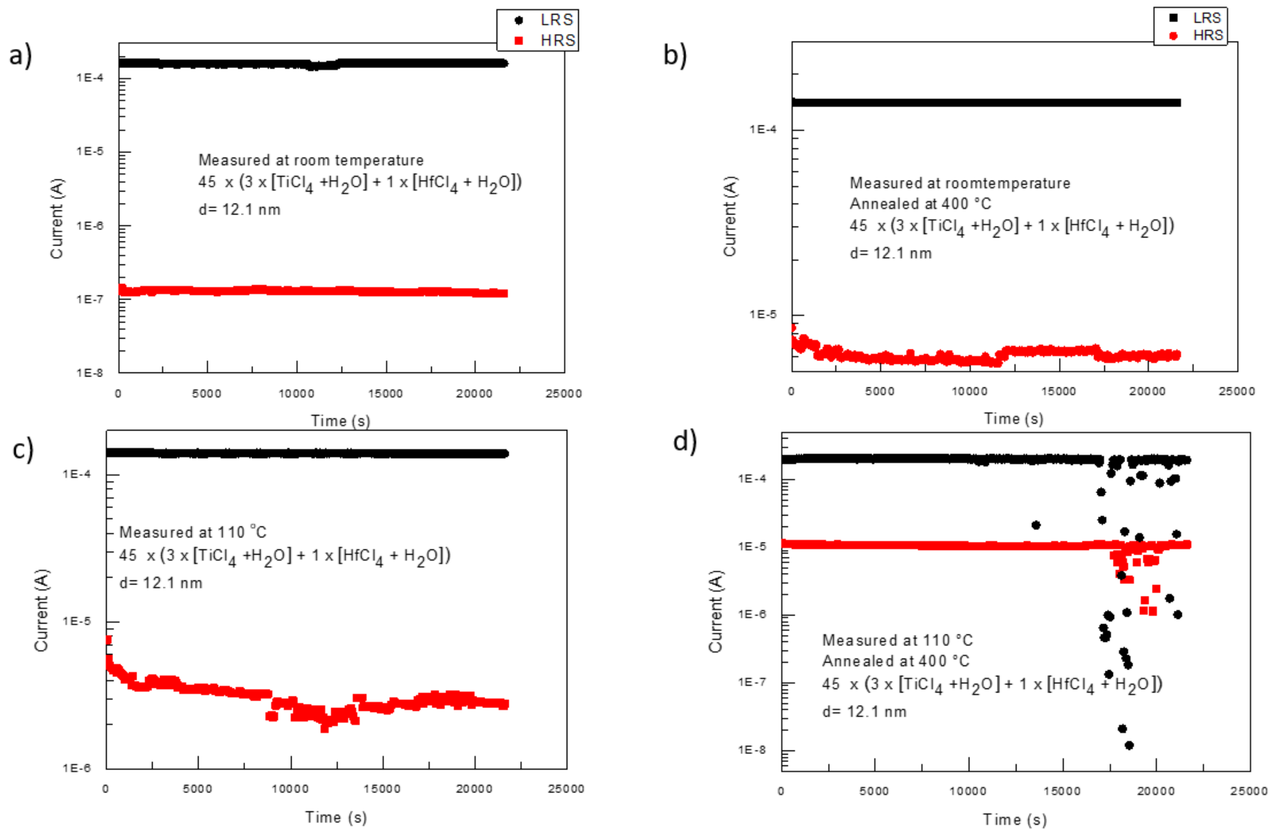

Fig. 18. Retention graphs at room temperature and 110 °C for both as-deposited (a, c) and annealed (b, d) samples with the ALD recipe of 45 × (3 × [$TiCl_4$ + H_2O] + 1 × [$HfCl_4$ + H_2O])

An additional retention measurement was carried out at 140 °C for the unannealed sample where the 3:1 deposition cycle ratio HfO_2:TiO_2 thin film was deposited using 80 supercycles (Fig. 19). The test showed good stability for both the HRS and LRS, although resistance in the HRS did decrease slightly over the course of the test.

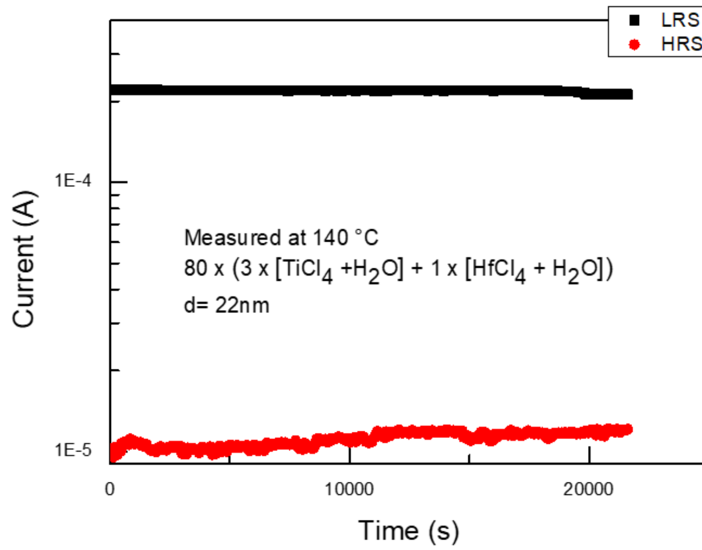

Fig. 19. Retention graph measured from the unannealed sample with the ALD recipe of 80 × (3 × [$TiCl_4$ + H_2O] + 1 × [$HfCl_4$ + H_2O]).

From table 1, if we look at the sample with the ALD recipe of 80 × (3 × [$TiCl_4$ + H_2O] + 1 × [$HfCl_4$ + H_2O]) we can see that from 1 ms to 100 µs the memory window width appears to decrease with the pulse length but suddenly increases with a pulse length of 10 µs and is still larger than previously with a pulse length of 1 µs. This suggest that there is no strong correlation between the pulse length of the applied voltage and the memory window width (I_{LRS}/I_{HRS}). However, the $\sigma/(I_{LRS}/I_{HRS})$ collum shows that as the pulse length decreases there is a higher chance that the device will not switch at all. This appears to be in line with literature. In Menzel et al. it was showed that in a certain range of voltages switching time depended heavily on the applied voltage but after increasing beyond a certain value this dependence decreased rapidly [55].

Sample	Pulse length (seconds)	$\mu(I_{LRS}/I_{HRS})$	$\sigma(I_{LRS}/I_{HRS})$	σ/μ
80 × (3 × [$TiCl_4$ + H_2O] + 1 × [$HfCl_4$ + H_2O]), Annealed, 22 nm	1 ms	22.73	8.25	0.36
	500 µs	18.45	7.81	0.42
	100 µs	16.51	4.52	0.27
	10 µs	31.43	17.47	0.56
	1 µs	23.85	14.73	0.62
80 × (3 × [$TiCl_4$ + H_2O] + 1 × [$HfCl_4$ + H_2O]), As-deposited, 22 nm	1 ms	8.25	2.30	0.28
	500 µs	8.66	3.86	0.45
	100 µs	5.50	1.57	0.29
	10 µs	7.71	8.93	1.16
	1 µs	5.21	7.17	1.38
45 × (3 × [TiCl4 + H2O] + 1 × [HfCl4 + H2O]), Annealed, 12.1 nm	1 ms	12.75	3.24	0.25
	500 µs	22.09	6.94	0.31
	100 µs	39.39	6.83	0.17
	10 µs	63.16	35.13	0.56
	1 µs	17.00	13.28	0.78

Table 1. Average memory window width (I_{LRS}/I_{HRS}) measured at different pulse lengths along with standard deviation ($\sigma(I_{LRS}/I_{HRS})$) for different samples and the coefficient of variation (σ/μ).

Due to time constraints only 3 samples underwent pulse length measurements. These objects were the annealed and unannealed samples with the ALD recipe of 80 × (3 × [$TiCl_4$ + H_2O] + 1 × [$HfCl_4$ + H_2O]), and the annealed sample with the ALD recipe of 45 × (3 × [$TiCl_4$ + H_2O] + 1 × [$HfCl_4$ + H_2O]). Fig 20. shows that when using pulse lengths of 160 ns resistive switching still occurs. However, reliably measuring the memory window width was not possible due to the noise present when using such short pulse lengths.

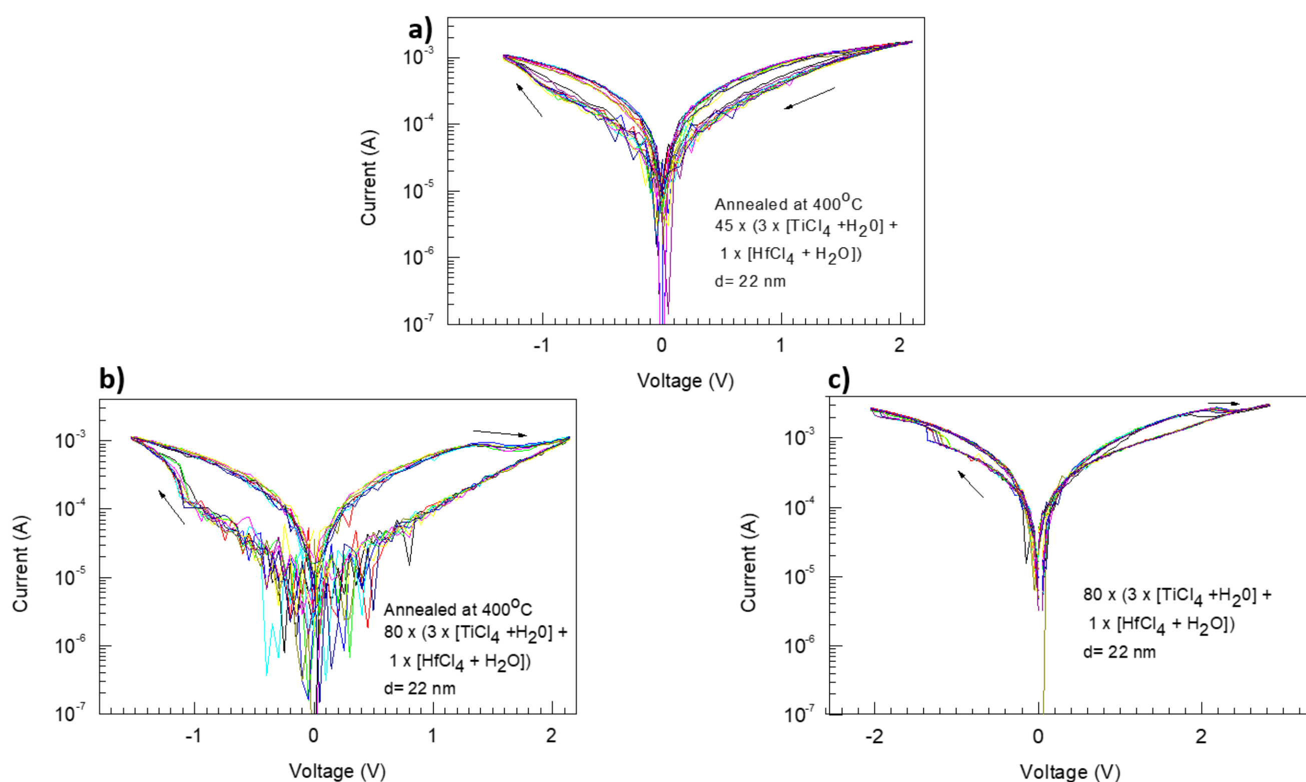

Fig. 20. I-V curves measured using 160 ns pulse widths for the annealed sample with the ALD recipe of 45 × (3 × [$TiCl_4$ + H_2O] + 1 × [$HfCl_4$ + H_2O]) (a), and the for both the annealed (b) and unannealed (c) samples with the ALD recipe of 80 × (3 × [$TiCl_4$ + H_2O] + 1 × [$HfCl_4$ + H_2O])

Repeatability test showed that samples where the 3:1 ALD cycle ratio HfO_2:TiO_2 thin film was deposited using 80 supercycles a repeatability of 6 out of 10 for the annealed sample and 4 out of 10 for the unannealed sample. The samples where the 3:1 ALD cycle ratio HfO_2:TiO_2 thin film was deposited using 45 supercycles showed a repeatability of 4 out of 10 for the annealed device and 6 out of 10 for the unannealed device.

12. Comparison

Table 2 shows and overview of the samples investigated in this work along with the gathered results. When comparing the samples where a HfO_2 thin film was deposited with the samples that had a HfO_2:TiO_2 thin film, we can see that the HfO_2 samples had higher switching voltages and poorer endurance performance. When comparing switching voltages in samples with a 3:1 deposition cycle ratio HfO_2:TiO_2 thin film, we can see that the thinner 12.1 nm thin films have lower SET switching voltages than the thicker 22 nm samples but higher RESET voltages. Additionally, the thinner films had worse retention characteristics. Annealing appears to have had a negative effect on endurance characteristics in all samples. All annealed samples performed worse than their unannealed counterparts in the endurance tests.

Table 2 also shows some samples taken from literature. In Lai et al. [56] resistive switching characteristics of Ag/TiO_2/Pt structures were studied. The 200 nm thick TiO_2 thin film was deposited using a sol-gel method. Endurance tests showed that the investigated material switched about 3800 times with an unstable memory window where some I_{LRS}/I_{HRS} values were almost 100 and others smaller than 3. Comparing these results with the unannealed HfO_2:TiO_2 sample with a 1:3 ALD cycle ratio deposited by 80 supercycles shows that the memory window is on average wider and more stable in the sample that was investigated in this work than those in the previously mentioned one. Additionally, it should be noted that our device switched in clockwise mode whereas the device studied by Lai et al. switched in counterclockwise mode.

Chen et al. [57] investigated samples with a TiN/HfO_2/Pt structure where the 30 nm thick HfO_2 thin film was deposited using tetrakis-(dimethylamido)-hafnium as an ALD precursor. The samples in the mentioned work have similar endurance performance as the unannealed samples with the 3:1 deposition ratio HfO_2:TiO_2 thin film. The switching voltages applied in the endurance test are also similar. Chen et al. applied a SET voltage of -1.5 V while samples in this work had a SET voltage of -1.7 V applied to them. RESET voltage was 2.0 V for Chen et al. samples and 2.2 V for our sample. When compared with the samples in this work retention was somewhat unstable in the samples that were investigated in Chen et al.

ALD recipe	Annealed	Thickness (nm)	V_{SET}(V)	V_{RESET}(V)	Endurance	Retention (20^4 sec at 110 °C)
80 × (3 × [$TiCl_4$ + H_2O] + 1 × [$HfCl_4$ + H_2O]),	Yes	22	-1.4 .. -0.95	1.05 .. 1.25	Unstable	Stable
80 × (3 × [$TiCl_4$ + H_2O] + 1 × [$HfCl_4$ + H_2O]),	No	22	-1.1 .. -0.85	1.1 .. 1.2	Stable	Stable
45 × (3 × [TiCl4 + H2O] + 1 × [HfCl4 + H2O])	Yes	12.1	-1.0 .. -0.8	1.55 .. 1.7	Unstable	Unstable
45 × (3 × [TiCl4 + H2O] + 1 × [HfCl4 + H2O])	No	12.1	-0.85 ..-0.65	0.9 .. 1.35	Stable	Unstable
120 × ($HfCl_4$ + H_2O)	Yes	10.1	-2.4 .. -1.2	2 .. 2.6	-	-
120 × ($HfCl_4$ + H_2O)	No	10.1	1.2 .. 1.4	-1.6 .. -1.1	Unstable	-
Structure						Retention (25 °C)
Ag/TiO_2/Pt, Lai et al. [56]	-	200	0.3 .. 0.5	-1.8 .. -1.6	Unstable (3000 cycles)	-
TiN/HfO_2/Pt, Chen et al.[57]	-	30	-1.0 .. -0.65	1.0 .. 1.4	stable (1000 cycles)	Unstable (10^4 sec)

Table 2. Overview of samples investigated in this work and the results gathered from them. Other samples from literature are also present for comparison.

13. Conclusion

In this work resistive switching was investigated in Pt/ HfO_2:TiO_2 /RuO_2 samples where the Pt top electrode was deposited using electron beam evaporation, the bottom RuO_2 electrode was deposited using magnetron sputtering and the HfO_2:TiO_2 thin film was deposited using atomic layer deposition. The metal precursors used in ALD were $HfCl_4$ and $TiCl_4$ and the oxidizing precursor was H_2O. N_2 was used for carrier gas. Different samples with varying HfO_2 to TiO_2 ratios were deposited. For each ratio there was two samples where in one of the samples the HfO_2:TiO_2 thin film was about twice as thick as in the other. Additionally, each of these sample also had corresponding duplicate that was annealed at 400 °C for a total of four samples per different HfO_2:TiO_2 ratio. GIXRD revealed that samples with a low Hf/(Hf+Ti) cation ratio demonstrated strong TiO_2 rutile reflexes while samples with high a high Hf/(Hf+Ti) demonstrated strong HfO_2 monoclinic reflexes. Intermediate Hf/(Hf+Ti) values showed the formation of a $HfTiO_4$ orthorhombic phase. Resistive switching measurements showed that samples with the ALD recipe of X × (3 × [$TiCl_4$ + H_2O] + 1 × [$HfCl_4$ + H_2O]) performed the best. In samples where X = 80 the measured thickness was 22 nm and in samples where X = 45 the measured thickness was 12.1 nm. Both the 22 nm and 12.1 nm samples demonstrated endurance of up to 3000 resistive switching cycles. However, the unannealed samples showed a more stable memory window. Retention measurements at 110 °C revealed that the 22 nm thick samples outperform the 12.1 nm thick samples. Measurements using different pulse lengths showed decreasing the pulse length of the applied voltage has a detrimental effect on resistive switching. Repeatability tests showed that the unannealed 22 nm thick sample had a repeatability of 4 out of 10 devices while the annealed sample had a repeatability of 6 out of 10 devices. The 12.1 nm thick samples showed a repeatability of 6 out of 10 devices for the unannealed sample and 4 out of 10 devices for the annealed sample. Based on this work it can be said that materials utilizing a Pt/ HfO_2:TiO_2/RuO_2 structure demonstrate good resistive switching properties and are therefore promising memory material candidates for use in non-volatile memory devices.

References

[1] H.-S. P. Wong *et al.*, ‘Metal–Oxide RRAM’, *Proc. IEEE*, vol. 100, no. 6, pp. 1951–1970, Jun. 2012, doi: 10.1109/JPROC.2012.2190369.

[2] Sungho Kim, Jiantao Zhou, and W. D. Lu, ‘Crossbar RRAM Arrays: Selector Device Requirements During Write Operation’, *IEEE Trans. Electron Devices*, vol. 61, no. 8, pp. 2820–2826, Aug. 2014, doi: 10.1109/TED.2014.2327514.

[3] Y.-C. Chen, H.-C. Yu, C.-Y. Huang, W.-L. Chung, S.-L. Wu, and Y.-K. Su, ‘Nonvolatile Bio-Memristor Fabricated with Egg Albumen Film’, *Sci. Rep.*, vol. 5, no. 1, p. 10022, May 2015, doi: 10.1038/srep10022.

[4] U. S. Bhansali *et al.*, ‘Metal-Free, Single-Polymer Device Exhibits Resistive Memory Effect’, *ACS Nano*, vol. 7, no. 12, pp. 10518–10524, Dec. 2013, doi: 10.1021/nn403873c.

[5] J. Merisalu *et al.*, ‘Engineering of atomic layer deposition process for titanium-aluminum-oxide based resistively switching medium’, *Mater. Sci. Eng. B*, vol. 282, p. 115797, Aug. 2022, doi: 10.1016/j.mseb.2022.115797.

[6] M. Lübben and I. Valov, ‘Active Electrode Redox Reactions and Device Behavior in ECM Type Resistive Switching Memories’, *Adv. Electron. Mater.*, vol. 5, no. 9, p. 1800933, Sep. 2019, doi: 10.1002/aelm.201800933.

[7] D. Yu *et al.*, ‘Multilevel resistive switching characteristics in Ag/SiO2/Pt RRAM devices’, in *2011 IEEE International Conference of Electron Devices and Solid-State Circuits*, Tianjin, China: IEEE, Nov. 2011, pp. 1–2. doi: 10.1109/EDSSC.2011.6117721.

[8] S. Gao *et al.*, ‘Resistive switching and conductance quantization in Ag/SiO2/indium tin oxide resistive memories’, *Appl. Phys. Lett.*, vol. 105, no. 6, p. 063504, Aug. 2014, doi: 10.1063/1.4893277.

[9] K.-L. Lin *et al.*, ‘Switching Mode and Mechanism in Binary Oxide Resistive Random Access Memory Using Ni Electrode’, *Jpn. J. Appl. Phys.*, vol. 52, no. 3R, p. 031801, Mar. 2013, doi: 10.7567/JJAP.52.031801.

[10] W. Guan, M. Liu, S. Long, Q. Liu, and W. Wang, ‘On the resistive switching mechanisms of Cu/ZrO2:Cu/Pt’, *Appl. Phys. Lett.*, vol. 93, no. 22, p. 223506, Dec. 2008, doi: 10.1063/1.3039079.

[11] S. Roy *et al.*, ‘Toward a Reliable Synaptic Simulation Using Al-Doped HfO_2 RRAM’, *ACS Appl. Mater. Interfaces*, vol. 12, no. 9, pp. 10648–10656, Mar. 2020, doi: 10.1021/acsami.9b21530.

[12] M. Ismail, U. Chand, C. Mahata, J. Nebhen, and S. Kim, ‘Demonstration of synaptic and resistive switching characteristics in W/TiO2/HfO2/TaN memristor crossbar array for bioinspired neuromorphic computing’, *J. Mater. Sci. Technol.*, vol. 96, pp. 94–102, Jan. 2022, doi: 10.1016/j.jmst.2021.04.025.

[13] S. C. Oh, H. Y. Jung, and H. Lee, ‘Effect of the top electrode materials on the resistive switching characteristics of TiO2 thin film’, *J. Appl. Phys.*, vol. 109, no. 12, p. 124511, Jun. 2011, doi: 10.1063/1.3596576.

[14] D.-H. Kwon *et al.*, ‘Atomic structure of conducting nanofilaments in TiO2 resistive switching memory’, *Nat. Nanotechnol.*, vol. 5, no. 2, pp. 148–153, Feb. 2010, doi: 10.1038/nnano.2009.456.

[15] C. Hu, M. D. McDaniel, A. Posadas, A. A. Demkov, J. G. Ekerdt, and E. T. Yu, ‘Highly Controllable and Stable Quantized Conductance and Resistive Switching Mechanism in Single-Crystal TiO_2 Resistive Memory on Silicon’, *Nano Lett.*, vol. 14, no. 8, pp. 4360–4367, Aug. 2014, doi: 10.1021/nl501249q.

[16] A. S. Sokolov *et al.*, 'Influence of oxygen vacancies in ALD HfO2-x thin films on non-volatile resistive switching phenomena with a Ti/HfO2-x/Pt structure', *Appl. Surf. Sci.*, vol. 434, pp. 822–830, Mar. 2018, doi: 10.1016/j.apsusc.2017.11.016.

[17] S. W. Ryu, S. Cho, J. Park, J. Kwac, H. J. Kim, and Y. Nishi, 'Effects of ZrO2 doping on HfO2 resistive switching memory characteristics', *Appl. Phys. Lett.*, vol. 105, no. 7, p. 072102, Aug. 2014, doi: 10.1063/1.4893568.

[18] Y. Wang *et al.*, 'Investigation of resistive switching in Cu-doped HfO $_2$ thin film for multilevel non-volatile memory applications', *Nanotechnology*, vol. 21, no. 4, p. 045202, Jan. 2010, doi: 10.1088/0957-4484/21/4/045202.

[19] C. Ye *et al.*, 'Enhanced resistive switching performance for bilayer HfO $_2$ /TiO $_2$ resistive random access memory', *Semicond. Sci. Technol.*, vol. 31, no. 10, p. 105005, Oct. 2016, doi: 10.1088/0268-1242/31/10/105005.

[20] Y. Chen, 'ReRAM: History, Status, and Future', *IEEE Trans. Electron Devices*, vol. 67, no. 4, pp. 1420–1433, Apr. 2020, doi: 10.1109/TED.2019.2961505.

[21] H. Wang and X. Yan, 'Overview of Resistive Random Access Memory (RRAM): Materials, Filament Mechanisms, Performance Optimization, and Prospects', *Phys. Status Solidi RRL – Rapid Res. Lett.*, vol. 13, no. 9, p. 1900073, Sep. 2019, doi: 10.1002/pssr.201900073.

[22] A. Wedig *et al.*, 'Nanoscale cation motion in TaOx, HfOx and TiOx memristive systems', *Nat. Nanotechnol.*, vol. 11, no. 1, pp. 67–74, Jan. 2016, doi: 10.1038/nnano.2015.221.

[23] C. Hermes *et al.*, 'Analysis of Transient Currents During Ultrafast Switching of TiO2 Nanocrossbar Devices', *IEEE Electron Device Lett.*, vol. 32, no. 8, pp. 1116–1118, Aug. 2011, doi: 10.1109/LED.2011.2156377.

[24] H. S. Nalwa, Ed., *Handbook of thin film materials*. San Diego: Academic Press, 2002.

[25] J. Niinistö *et al.*, 'Atomic Layer Deposition of HfO $_2$ Thin Films Exploiting Novel Cyclopentadienyl Precursors at High Temperatures', *Chem. Mater.*, vol. 19, no. 13, pp. 3319–3324, Jun. 2007, doi: 10.1021/cm0626583.

[26] S. K. Kim, S. Hoffmann-Eifert, M. Reiners, and R. Waser, 'Relation Between Enhancement in Growth and Thickness-Dependent Crystallization in ALD TiO[sub 2] Thin Films', *J. Electrochem. Soc.*, vol. 158, no. 1, p. D6, 2011, doi: 10.1149/1.3507258.

[27] P. Eiamchai, P. Chindaudom, A. Pokaipisit, and P. Limsuwan, 'A spectroscopic ellipsometry study of TiO2 thin films prepared by ion-assisted electron-beam evaporation', *Curr. Appl. Phys.*, vol. 9, no. 3, pp. 707–712, May 2009, doi: 10.1016/j.cap.2008.06.011.

[28] Y. Wang, Z. Lin, X. Cheng, H. Xiao, F. Zhang, and S. Zou, 'Study of HfO2 thin films prepared by electron beam evaporation', *Appl. Surf. Sci.*, vol. 228, no. 1–4, pp. 93–99, Apr. 2004, doi: 10.1016/j.apsusc.2003.12.028.

[29] M. Ohring, *Materials science of thin films: deposition and structure*, 2nd ed. San Diego, CA: Academic Press, 2002.

[30] L. W. Martin, Y.-H. Chu, and R. Ramesh, 'Advances in the growth and characterization of magnetic, ferroelectric, and multiferroic oxide thin films', *Mater. Sci. Eng. R Rep.*, vol. 68, no. 4–6, pp. 89–133, May 2010, doi: 10.1016/j.mser.2010.03.001.

[31] K. S. SreeHarsha, *Principles of physical vapor deposition of thin films*, 1st ed. Amsterdam ; Boston: Elsevier, 2006.

[32] M. Birkholz, P. F. Fewster, and C. Genzel, *Thin film analysis by X-ray scattering*. Weinheim: Wiley-VCH, 2006.

[33] J. Aarik, A. Aidla, H. Mändar, T. Uustare, K. Kukli, and M. Schuisky, 'Phase transformations in hafnium dioxide thin films grown by atomic layer deposition at high temperatures', *Appl. Surf. Sci.*, vol. 173, no. 1–2, pp. 15–21, Mar. 2001, doi: 10.1016/S0169-4332(00)00859-X.

[34] G. D. Wilk, R. M. Wallace, and J. M. Anthony, 'High-κ gate dielectrics: Current status and materials properties considerations', *J. Appl. Phys.*, vol. 89, no. 10, pp. 5243–5273, May 2001, doi: 10.1063/1.1361065.

[35] J. McPherson, J.-Y. Kim, A. Shanware, and H. Mogul, 'Thermochemical description of dielectric breakdown in high dielectric constant materials', *Appl. Phys. Lett.*, vol. 82, no. 13, pp. 2121–2123, Mar. 2003, doi: 10.1063/1.1565180.

[36] J. Robertson, 'High dielectric constant oxides', *Eur. Phys. J. Appl. Phys.*, vol. 28, no. 3, pp. 265–291, Dec. 2004, doi: 10.1051/epjap:2004206.

[37] H. Kim, P. C. McIntyre, and K. C. Saraswat, 'Effects of crystallization on the electrical properties of ultrathin HfO2 dielectrics grown by atomic layer deposition', *Appl. Phys. Lett.*, vol. 82, no. 1, pp. 106–108, Jan. 2003, doi: 10.1063/1.1533117.

[38] L. Zhao *et al.*, 'Multi-level control of conductive nano-filament evolution in HfO_2 ReRAM by pulse-train operations', *Nanoscale*, vol. 6, no. 11, pp. 5698–5702, 2014, doi: 10.1039/C4NR00500G.

[39] W. Banerjee, A. Kashir, and S. Kamba, 'Hafnium Oxide (HfO_2) – A Multifunctional Oxide: A Review on the Prospect and Challenges of Hafnium Oxide in Resistive Switching and Ferroelectric Memories', *Small*, vol. 18, no. 23, p. 2107575, Jun. 2022, doi: 10.1002/smll.202107575.

[40] S. Brivio, S. Spiga, and D. Ielmini, 'HfO_2-based resistive switching memory devices for neuromorphic computing', *Neuromorphic Comput. Eng.*, vol. 2, no. 4, p. 042001, Dec. 2022, doi: 10.1088/2634-4386/ac9012.

[41] M. H. Park, Y. H. Lee, T. Mikolajick, U. Schroeder, and C. S. Hwang, 'Review and perspective on ferroelectric HfO2-based thin films for memory applications', *MRS Commun.*, vol. 8, no. 3, pp. 795–808, Sep. 2018, doi: 10.1557/mrc.2018.175.

[42] P. Y. Simons and F. Dachille, 'The structure of TiO_2 II, a high-pressure phase of TiO_2', *Acta Crystallogr.*, vol. 23, no. 2, pp. 334–336, Aug. 1967, doi: 10.1107/S0365110X67002713.

[43] L. Palmisano, F. Parrino, and G. Korotcenkov, Eds., *Titanium dioxide (tio2) and its applications*, 1st ed. Cambridge: Elsevier, 2021.

[44] J. Aarik, A. Aidla, A.-A. Kiisler, T. Uustare, and V. Sammelselg, 'Effect of crystal structure on optical properties of TiO2 films grown by atomic layer deposition', *Thin Solid Films*, vol. 305, no. 1–2, pp. 270–273, Aug. 1997, doi: 10.1016/S0040-6090(97)00135-1.

[45] A. P. Alekhin, S. A. Gudkova, A. M. Markeev, A. S. Mitiaev, A. A. Sigarev, and V. F. Toknova, 'Structural properties of the titanium dioxide thin films grown by atomic layer deposition at various numbers of reaction cycles', *Appl. Surf. Sci.*, vol. 257, no. 1, pp. 186–191, Oct. 2010, doi: 10.1016/j.apsusc.2010.06.061.

[46] W.-J. Lee and M.-H. Hon, 'Space-Limited Crystal Growth Mechanism of TiO_2 Films by Atomic Layer Deposition', *J. Phys. Chem. C*, vol. 114, no. 15, pp. 6917–6921, Apr. 2010, doi: 10.1021/jp911210q.

[47] J. Aarik, A. Aidla, T. Uustare, and S. Väino, ‘Morphology and structure of T i O 2 thin films grown by atomic layer deposition’, *J. Cryst. Growth*, vol. 148, no. 3, pp. 286–275.

[48] K. Kukli *et al.*, ‘Atomic Layer Deposition of Titanium Oxide from TiI4 and H2O2’, *Chem. Vap. Depos.*, vol. 6, no. 6, pp. 303–310, Nov. 2000, doi: 10.1002/1521-3862(200011)6:6<303::AID-CVDE303>3.0.CO;2-J.

[49] B. D. Piercy, C. Z. Leng, and M. D. Losego, ‘Variation in the density, optical polarizabilities, and crystallinity of TiO2 thin films deposited via atomic layer deposition from 38 to 150 °C using the titanium tetrachloride-water reaction’, *J. Vac. Sci. Technol. Vac. Surf. Films*, vol. 35, no. 3, p. 03E107, May 2017, doi: 10.1116/1.4979047.

[50] B. J. Choi *et al.*, ‘Resistive switching mechanism of TiO2 thin films grown by atomic-layer deposition’, *J. Appl. Phys.*, vol. 98, no. 3, p. 033715, Aug. 2005, doi: 10.1063/1.2001146.

[51] P. M. Zagwijn *et al.*, ‘Novel Batch Titanium Nitride CVD Process for Advanced Metal Electrodes’, *ECS Trans.*, vol. 13, no. 1, pp. 459–464, Oct. 2008, doi: 10.1149/1.2911530.

[52] J. Gatineau, K. Yanagita, and C. Dussarrat, ‘A new RuO4 solvent solution for pure ruthenium film depositions’, *Microelectron. Eng.*, vol. 83, no. 11–12, pp. 2248–2252, Nov. 2006, doi: 10.1016/j.mee.2006.10.013.

[53] T. Arroval, L. Aarik, R. Rammula, V. Kruusla, and J. Aarik, ‘Effect of substrate-enhanced and inhibited growth on atomic layer deposition and properties of aluminum–titanium oxide films’, *Thin Solid Films*, vol. 600, pp. 119–125, Feb. 2016, doi: 10.1016/j.tsf.2016.01.024.

[54] J. J. Friel and C. E. Lyman, ‘Tutorial Review: X-ray Mapping in Electron-Beam Instruments’, *Microsc. Microanal.*, vol. 12, no. 01, pp. 2–25, Feb. 2006, doi: 10.1017/S1431927606060211.

[55] S. Menzel, U. Böttger, M. Wimmer, and M. Salinga, ‘Physics of the Switching Kinetics in Resistive Memories’, *Adv. Funct. Mater.*, vol. 25, no. 40, pp. 6306–6325, Oct. 2015, doi: 10.1002/adfm.201500825.

[56] C.-H. Lai, C.-H. Chen, and T.-Y. Tseng, ‘Resistive switching behavior of sol–gel deposited TiO 2 thin films under different heating ambience’, *Surf. Coat. Technol.*, vol. 231, pp. 399–402, Sep. 2013, doi: 10.1016/j.surfcoat.2012.05.045.

[57] X. Chen, W. Hu, Y. Li, S. Wu, and D. Bao, ‘Complementary resistive switching behaviors evolved from bipolar TiN/HfO2/Pt device’, *Appl. Phys. Lett.*, vol. 108, no. 5, p. 053504, Feb. 2016, doi: 10.1063/1.4941287.

Non-exclusive licence to reproduce the thesis and make the thesis public

I, **Toomas Daniel Viskus**

1. grant the University of Tartu a free permit (non-exclusive licence) to

reproduce, for the purpose of preservation, including for adding to the DSpace digital archives until the expiry of the term of copyright, my thesis

"Resistive switching in HfO_2 - TiO_2 thin films"

supervised by **PhD Kaupo Kukli and MSc Joonas Merisalu**

2. I grant the University of Tartu a permit to make the thesis specified in point 1 available to the public via the web environment of the University of Tartu, including via the DSpace digital archives, under the Creative Commons licence CC BY NC ND 4.0, which allows, by giving appropriate credit to the author, to reproduce, distribute the work and communicate it to the public, and prohibits the creation of derivative works and any commercial use of the work until the expiry of the term of copyright.

3. I am aware of the fact that the author retains the rights specified in points 1 and 2.

4. I confirm that granting the non-exclusive licence does not infringe other persons' intellectual property rights or rights arising from the personal data protection legislation.

/Signed digitally/

Toomas Daniel Viskus

30.05.2024